



Published in final edited form as:

Nat Neurosci. 2017 December ; 20(12): 1694–1707. doi:10.1038/s41593-017-0013-0.

***Arid1b* haploinsufficiency disrupts cortical interneuron development and mouse behavior**

Eui-Man Jung¹, Jeffrey Jay Moffat¹, Jinxu Liu², Shashank Manohar David², Channabasavaiah Gurumurthy¹, and Woo-Yang Kim^{1,*}

¹Department of Developmental Neuroscience, Munroe-Meyer Institute, University of Nebraska Medical Center, Omaha, NE 68198

²Department of Pharmacology, Creighton University, Omaha, NE 68178

Abstract

Haploinsufficiency of the *AT-rich interactive domain 1B (ARID1B)* gene causes autism spectrum disorder (ASD) and intellectual disability, however, the neurobiological basis for this is unknown. Here, we generated *Arid1b* knockout mice and examined heterozygotes to model human patients. *Arid1b* heterozygous mice showed a decreased number of cortical GABAergic interneurons and reduced proliferation of interneuron progenitors in the ganglionic eminence. *Arid1b* haploinsufficiency also led to an imbalance between excitatory and inhibitory synapses in the cerebral cortex. Furthermore, we found that *Arid1b* haploinsufficiency suppressed histone H3 lysine 9 acetylation (H3K9Ac) overall, and in particular reduced H3K9Ac of the *Pvalb* promoter, resulting in decreased transcription. *Arid1b* heterozygous mice exhibited abnormal cognitive and social behavior, which was rescued by treatment with a positive allosteric GABA_A receptor modulator. Our results demonstrate a critical role for the *Arid1b* gene in interneuron development and behavior, and provide insight into the pathogenesis of ASD and intellectual disability.

Keywords

Arid1b; haploinsufficiency; autism spectrum disorder; intellectual disability; interneuron; parvalbumin; GABA

Users may view, print, copy, and download text and data-mine the content in such documents, for the purposes of academic research, subject always to the full Conditions of use: http://www.nature.com/authors/editorial_policies/license.html#terms

*Correspondence to: Woo-Yang Kim, Ph.D., wooyang.kim@unmc.edu, PHONE: 1-402-559-1337, FAX: 1-402-559-2256.

Note: Any Supplementary Information and Source Data files are available in the online version of the paper.

AUTHOR CONTRIBUTIONS

E.J. and W.K. designed, performed and analyzed the experiments, and wrote the paper. J.J.M., C.G. and J.L. performed the experiments. S.D. designed and analyzed the experiments. W.K. conceived and supervised the study.

COMPETING FINANCIAL INTERESTS

Authors declare no competing financial interests.

Data availability

The data that support the findings of this study are available from the corresponding author upon reasonable request.

INTRODUCTION

Autism spectrum disorder (ASD) impairs the ability of individuals to communicate and interact with others. Approximately 75% of individuals with ASD also have intellectual disability, which is characterized by significant limitations in cognitive functions and adaptive behaviors¹. While ASD and intellectual disability are currently defined using behavioral criteria, little is known about the neuropathogenesis of these conditions. There are no pharmacological and/or genetic treatments to prevent ASD or intellectual disability, and current treatment options focus on behavioral management and educational and physical therapies. Development of therapeutic tools requires identification and targeting of causative factors.

Recent genetic studies have reported that haploinsufficiency of *AT-rich interactive domain 1B* (*ARID1B*) causes ASD and non-syndromic and syndromic intellectual disability including Coffin-Siris syndrome²⁻⁴. However, the neurobiological function of *ARID1B* during brain development is unknown. *ARID1B* is a component of the human Brg1/Brm associated factor (BAF) chromatin remodeling complex and controls gene expression by facilitating DNA access for transcription factors⁵. The *ARID1B* protein binds to DNA sequences via its AT-rich DNA-binding domain. Chromatin remodeling as an epigenetic mechanism is critically linked to ASD and intellectual disability⁶.

GABAergic interneurons play an important role in neural circuitry and emotional and cognitive behaviors⁷. The balance of excitatory and inhibitory neurotransmission is essential for controlling memory and emotional behaviors and is disrupted in ASD and intellectual disability^{8,9}. Reduction of inhibitory signaling is particularly involved in ASD-like behaviors in human and mouse models of ASD^{10,11}. Proper positioning and differentiation of interneurons during brain development are important for establishing anatomical and functional circuitry necessary for normal cognition¹².

To investigate the neurobiological role of *Arid1b*, we have generated *Arid1b* knockout mice. *Arid1b* heterozygous mice in particular could be an excellent model for disorders related to *ARID1B* haploinsufficiency. We found that *Arid1b* haploinsufficiency leads to an excitation/inhibition imbalance by reducing the number of GABAergic interneurons in the cerebral cortex. Furthermore, we showed that treatment with a GABA_AR positive allosteric modulator rescues ASD-like behavior and cognitive dysfunction in *Arid1b* heterozygous mice, suggesting an association between lower numbers of GABAergic interneurons and behavioral outcomes. Our findings suggest a pathogenic mechanism for ASD and intellectual disability.

RESULTS

Altered number and distribution of cortical interneurons in *Arid1b*^{+/-} mice

Arid1b knockout mice were generated using ES cells that contain a 'knockout-first' design¹³ of the targeted *Arid1b* allele harboring LoxP sites flanking exon 5 (Supplementary Fig. 1). We first examined the lamination patterns of excitatory pyramidal neurons in P28 and P91 wild-type control (*Arid1b*^{+/+}) and *Arid1b*^{+/-} brains. *Arid1b*^{+/-} cortices showed grossly

normal CUX1 and TBR1 layering patterns, comparable to control cortices (Supplementary Fig. 2 and Supplementary Table 1). Furthermore, we observed no significant changes in the densities of CUX1-, TBR1-, or NeuN-positive neurons as well as Olig2-positive oligodendrocytes or GFAP-positive astrocytes in *Arid1b*^{+/-} cortices (Supplementary Fig. 2).

Next, we assessed the positioning and density of inhibitory interneurons in *Arid1b*^{+/-} brains. Interestingly, GABA- and parvalbumin-positive neuron densities were decreased in *Arid1b*^{+/-} cortices compared with controls at P91 (Fig. 1a–d and Supplementary Table 1). We also found that interneurons were abnormally positioned in *Arid1b*^{+/-} cortical layers. Other regions, such as the amygdala, thalamus, and hippocampus in *Arid1b*^{+/-} brains at P28 and P91, also showed reduced numbers of GABA- and parvalbumin-positive interneurons (Supplementary Fig. 3). However, we found no change in the densities of somatostatin-, calbindin- and calretinin-positive cells in *Arid1b*^{+/-} cortices compared with controls (Supplementary Fig. 4 and Supplementary Table 1). Additionally, we assessed interneuron numbers in conditional *Arid1b*^{lox/+} mice after crossing with the *Dlx5/6-Cre-IRES-EGFP*¹⁴ or *Nkx2.1-Cre*¹⁵ mouse line. The densities of GABA- and parvalbumin-positive neurons were decreased in *Arid1b*^{loxP/+}; *Dlx5/6-Cre-IRES-EGFP* and *Arid1b*^{loxP/+}; *Nkx2.1-Cre* cortices compared with *Arid1b*^{+/+}; *Dlx5/6-Cre-IRES-EGFP* and *Arid1b*^{+/+}; *Nkx2.1-Cre* controls (Supplementary Fig. 5a–g). Conditional deletion of *Arid1b* did not lead to significant changes in body weight in mutant mice (Supplementary Fig. 5h). The reduced cortical interneurons in postnatal *Arid1b*^{+/-} mice led us to examine whether the abnormalities observed in mutants began during embryonic development. The number of EGFP-positive interneurons was significantly reduced in *Arid1b*^{+/-}; *Dlx5/6-Cre-IRES-EGFP* cortices at E12.5, E14.5, E16.5 and E18.5 compared with controls (Fig. 1e–h and Supplementary Fig. 6). Taken together, these results show that *Arid1b* haploinsufficiency leads to a substantial reduction in cortical interneurons.

Development of cortical interneurons in *Arid1b*^{+/-} mice

Interneuron migration plays an important role in determining the quantity and positioning of cortical interneurons. Using time-lapse imaging of EGFP-positive interneurons on cortical slices from E13.5 control (*Arid1b*^{+/+}; *Dlx5/6-Cre-IRES-EGFP*) and *Arid1b*^{+/-}; *Dlx5/6-Cre-IRES-EGFP* mice, we found no significant differences in migration speeds in *Arid1b*^{+/-} interneurons compared with controls (Fig. 2a–c). We then examined the proliferation of *Arid1b*^{+/-} ventral progenitors in the medial ganglionic eminence (MGE), which is the primary source of cortical interneurons in the developing brain. The number of proliferating cells positive to phosphorylated histone-H3 or BrdU was decreased in *Arid1b*^{+/-} MGEs compared with controls (Fig. 2d, e). Next, we assessed apoptotic cells in control and *Arid1b*^{+/-} MGEs and lateral ganglionic eminences (LGEs) by cleaved caspase-3 and TUNEL staining. The numbers of cleaved caspase-3-positive and TUNEL-positive cells were increased in *Arid1b*^{+/-} MGEs and LGEs (Fig. 2f, g). The increased dying cells in the MGE were progenitors as they were double-positive to phosphorylated-histone H3 and cleaved caspase-3 (Fig. 2h). To further confirm our observations, we assessed cell death in cultured MGE progenitors. The number of proliferating progenitors labeled with BrdU was decreased in *Arid1b*^{+/-} cultures compared with controls while the numbers of cleaved caspase-3- or TUNEL-positive cells were increased (Fig. 2i–l). These results suggest that

Arid1b haploinsufficiency reduces the number of cortical interneurons by inhibiting proliferation and promoting apoptosis of GE progenitors during brain development. We examined expression of the components in Wnt/ β -catenin signaling, which plays an important role in ventral progenitor proliferation and development. The protein levels of β -catenin and its target Cyclin D1 were decreased in *Arid1b* knockout ventral telencephalons in a gene dose-dependent manner while the level of phospho- β -catenin was increased (Supplementary Fig. 7a, b). The transcript levels of *Ctnnb1* and its target genes as well as *Wnt* family genes were mostly downregulated in *Arid1b* knockout samples (Supplementary Fig. 7c, d).

We investigated neurite morphology of *Arid1b* heterozygous interneurons by tracing EGFP-positive cells in P91 *Arid1b^{+/-};Dlx5/6-Cre-IRES-EGFP* mice. The length and number of *Arid1b^{+/-}* interneuron neurites were decreased in *Arid1b^{+/-};Dlx5/6-Cre-IRES-EGFP* mice compared with *Arid1b^{+/+};Dlx5/6-Cre-IRES-EGFP* mice (Supplementary Fig. 8).

Synaptic structure and function in *Arid1b^{+/-}* mice

The altered number and morphology of interneurons suggest that the *Arid1b^{+/-}* cortex may have abnormal neuronal connectivity. Indeed, the numbers of inhibitory synaptic puncta positive to VIAAT and glutamic acid decarboxylase 2 (GAD2) were decreased in *Arid1b^{+/-}* cortices compared with control numbers (Fig. 3a, b). However, we found no change in the number of excitatory synaptic puncta positive to vesicular glutamate transporter 1 (VGluT1, Slc17a7) in *Arid1b^{+/-}* cortices. Also, we observed no changes in the number of excitatory synapses assessed by colocalized puncta of the postsynaptic marker, disks large homolog 4 (PSD95), and presynaptic marker VGluT1 in P91 *Arid1b^{+/-}* cortices (Supplementary Fig. 9). We measured the ratio of VGluT1-positive to VIAAT-positive synapses in cortical layers 2/3e. *Arid1b^{+/-}* cortices exhibited a higher ratio of excitatory to inhibitory synapses than controls (Fig. 3c), suggesting excitatory/inhibitory (E/I) imbalance. Additionally, using real-time PCR we found that the levels of *Gad1* and *Gad2* mRNAs were downregulated in *Arid1b^{+/-}* cortices (Fig. 3d, Supplementary Fig. 7e). The mRNA levels of inhibitory postsynaptic markers *Gphn* and *Arhgef9* were decreased in *Arid1b^{+/-}* cortices while the levels of excitatory markers *Slc17a7* and *Dlg4* were not changed in *Arid1b^{+/-}* cortices compared with control levels. However, *Arid1b^{-/-}* cortices showed reduced levels of *Slc17a7* and *Dlg4* compared with wild type and *Arid1b^{+/-}* samples (Supplementary Fig. 7e). GABA receptor levels were not changed in *Arid1b^{+/-}* samples, but decreased in *Arid1b^{-/-}* samples (Fig. 3d, Supplementary Fig. 7e). The protein level of GAD1 was also decreased in *Arid1b^{+/-}* cortices (Fig. 3e, f).

To determine if *Arid1b* haploinsufficiency affects excitatory and inhibitory neurotransmission, we performed whole-cell recordings on pyramidal neurons in cortical slices. No changes were found in the frequency, inter-event interval, and amplitude of mEPSCs between control and *Arid1b^{+/-}* neurons (Fig. 4a, Supplementary Fig. 10a). In contrast, the frequency of mIPSC was decreased in *Arid1b^{+/-}* cortical neurons compared with controls (Fig. 4b, Supplementary Fig. 10b). The cumulative fraction curves revealed an increased inter-event interval in *Arid1b^{+/-}* cortical neurons. We further examined the morphology of inhibitory synapses in *Arid1b^{+/-}* mice. *Arid1b^{+/-}* cortices at P91 showed an

increase in the cleft width of symmetric synapses, compared with controls, whereas they had the decreased length of postsynaptic density (Fig. 4c, d). Together, our data show that *Arid1b* haploinsufficiency results in E/I imbalance via abnormal formation and transmission of inhibitory synapses.

***Arid1b* haploinsufficiency disrupts epigenetic programming**

We assessed histone H3 acetylation and methylation, essential for transcription regulation, in *Arid1b*^{+/-} brains. We found that the levels of transcriptional activators, histone H3 acetylation at Lysine 9 (H3K9ac) and histone H3 trimethylation at Lysine 4 (H3K4me3), were decreased in *Arid1b*^{+/-} cortices, compared with control levels, while the level of the transcriptional repressor, histone H3 trimethylation at Lysine 27 (H3K27me3), was increased (Fig. 5a, b, Supplementary Fig. 7a, b). *Arid1b*^{-/-} cortices contained H3K9ac and H3K4me3 levels similar to *Arid1b*^{+/-} samples, but showed the increased level of H3K27me3 (Supplementary Fig. 7a, b). The levels of all histone subunits such as H1, H2A, H3, and H4 showed no changes between *Arid1b*^{+/-} and control samples (Fig 5a, c). These results suggested that *Arid1b* haploinsufficiency might suppress the activity of histone acetyltransferases (HATs) or enhance the activity of histone deacetylases (HDACs) in the brain. However, HAT and HDAC assays showed no differences in the activity of the histone modifiers between control and *Arid1b*^{+/-} cortices (Fig. 5d). H3K9 acetylation can be regulated by the amounts of HATs or HDACs as well as by the activity. Compared with controls, *Arid1b*^{+/-} cortices showed no changes in mRNA levels of several HATs and HDACs including *Crebbp* (*Cbp*), *Ep300*, *Kat2b* (*Pcaf*), *Kat5*, *Hdac1*, *Hdac2*, *Hdac3*, and *Hdac4* (Fig. 5e). We further assessed the levels of histone deacetylase 4 localized in the nucleus and cytosol because nuclear accumulation of the protein is associated with neuronal development. Again, there was no change in nuclear accumulation of this histone deacetylase between *Arid1b*^{+/-} and control cortices (Fig. 5f). Interestingly, the protein level of acetyl-CREB-binding protein (CBP), which enhances HAT function, was decreased in *Arid1b*^{+/-} cortices while the levels of CBP and PCAF were not altered (Fig 5g, h, Supplementary Fig. 7a, b). However, the level of PCAF in *Arid1b*^{-/-} cortices was decreased compared with control and *Arid1b*^{+/-} sample levels (Supplementary Fig. 7a, b). Next, we examined the physical association of H3K9ac and HATs. ARID1B could potentially mediate the interaction between HATs and histone H3. Indeed, using Co-IP we found decreased levels of CBP and PCAF bound to H3K9ac in *Arid1b*^{+/-} cortices compared with controls (Fig 5i, j). We verified the reduced binding of the HATs and histone H3 using another method, the proximity-dependent biotin identification (BioID2)¹⁶. Similar to the Co-IP results, the levels of CBP and PCAF bound to histone H3 were decreased in *Arid1b*^{+/-} samples (Fig. 5k, l). These data suggest that ARID1B may function as a bridge between histone H3 and HATs.

Arid1b haploinsufficiency led to decreased levels of *Pvalb* and *Ntrk2* transcripts (Fig. 5m). Thus, we investigated whether ARID1B regulates histone H3 acetylation in the *Pvalb* promoter using the ChIP-qPCR assay. The upstream regions adjacent to the transcription start site of the first exon were analyzed (Fig. 5n). We found that ARID1B bound to the *Pvalb* promoter around the transcription start site in control cortices (Fig. 5o, p). ARID1B binding to *Pvalb* promoter regions 1 and 2 was decreased in *Arid1b*^{+/-} cortices, whereas

Pvalb promoter region 3 binding was not changed. To verify that ARID1B binding at the *Pvalb* promoter causes expression changes via epigenetic mechanisms, we performed other sets of ChIP-qPCR experiments. First, we included two negative controls. We examined whether ARID1B binds to a distal intergenic or an intron region of the *Pvalb* gene. We found no binding of ARID1B to the regions (Supplementary Fig. 11a, b). Second, we performed the ChIP-PCR to investigate two promoter regions of excitatory neuron-relevant genes, *Slc17a7* and *Dlg4*. The mRNA levels of these genes were not changed in *Arid1b*^{+/-} cortices compared with control levels (Fig. 3d and Supplementary Fig. 7e). We found that ARID1B bound to the *Slc17a7* and *Dlg4* promoters around transcription start sites, but the levels of ARID1B binding were not different between control and *Arid1b*^{+/-} cortices (Supplementary Fig. 11c, d). Finally, we performed two more sets of the ChIP-qPCR assay examining ARID1B binding to the promoters of inhibitory neuron-relevant *Gad1* and *Slc32a1* genes. Expression of these genes was downregulated in *Arid1b*^{+/-} cortices (Fig. 3d and Supplementary Fig. 7e). ARID1B was associated with *Gad1* and *Slc32a1* promoter regions in wild type and *Arid1b*^{+/-} cortical tissues (Supplementary Fig. 11e, f). The levels of ARID1B binding to the promoters were decreased in *Arid1b*^{+/-} samples, compared with the levels in controls. These results suggest an adverse effect of *Arid1b* haploinsufficiency on gene expression related to interneuron development.

Next, we examined an association of H3K9ac with the *Pvalb* promoter in *Arid1b*^{+/-} cortices. H3K9ac bound to the *Pvalb* promoter regions, but the levels of H3K9ac in *Pvalb* promoter regions 1 and 2 were decreased in *Arid1b*^{+/-} cortices, similar to the ARID1B interaction pattern to the *Pvalb* promoter (Fig. 5q, r). To verify that the reduced H3K9ac signature and transcription were specific to the *Pvalb* gene in parvalbumin cells, we measured the level of H3K9ac binding to promoters of *Syt2* and *Ppargc1a*, which are specifically expressed in parvalbumin interneurons, but not in other types of interneurons or excitatory neurons¹⁷⁻¹⁹. We found that the *Syt2* and *Ppargc1a* mRNA levels were not significantly altered in *Arid1b*^{+/-} cortices compared with the control level (Supplementary Fig. 12a). The ChIP-qPCR assay showed that H3K9ac bound to *Syt2* and *Ppargc1a* promoters in control and *Arid1b*^{+/-} cortices (Supplementary Fig. 12b-g). The levels of H3K9ac binding to the promoters were not changed in *Arid1b*^{+/-} samples. These results suggest that by controlling physical access of histone modifiers and subsequently creating favorable and relaxed chromatin environments, ARID1B may facilitate *Pvalb* gene transcription. Thus, we tested if ARID1B haploinsufficiency interferes with the initiation of *Pvalb* gene transcription. We performed the ChIP-qPCR assay using an antibody to phosphorylated (Ser5)-carboxy-terminal domain (CTD) of RNA polymerase II. The CTD is distinctly phosphorylated at the serine 5 residue only during transcription initiation. The levels of phospho-CTD (Ser5) associated with the *Pvalb* promoter were decreased in *Arid1b*^{+/-} cortices compared with control levels (Fig. 5s, t), indicating that transcription initiation of the *Pvalb* gene was suppressed in *Arid1b*^{+/-} cortices. Transcription initiation of the *Ntrk2* gene was similarly suppressed in *Arid1b*^{+/-} cortices (Supplementary Fig. 11g-i). In contrast, the levels of phospho-CTD (Ser5) in the *Syt2* promoter were not different between control and *Arid1b*^{+/-} cortices (Supplementary Fig. 12h, i). Together, our data suggest that ARID1B regulates *Pvalb* gene expression by recruiting HATs to histone molecules on the target promoter and facilitating chromatin remodeling for transcription initiation control.

Abnormal cognitive and social behavior in *Arid1b*^{+/-} mice

To address the functional relevancy of the morphological and biochemical changes in *Arid1b*^{+/-} mice, we examined cognitive, social and emotional behaviors that model clinical features of ASD and intellectual disability. We first performed the Morris water maze test. During the acquisition phase, the differences in escape latency time between the two genotypes continued in a consistent manner after 4 days of training (Fig. 6a), indicating the capacity for spatial learning in *Arid1b*^{+/-} mice is limited, rather than delayed. In the probe trial, *Arid1b*^{+/-} mice crossed the platform location fewer times, whereas both control and *Arid1b*^{+/-} mice showed no differences in swimming distances and swimming speeds (Fig. 6b, c). In the T-maze test, *Arid1b*^{+/-} mice exhibited an impaired spatial reference memory (Fig. 6d). We also assessed recognition memory using a novel object recognition test. While control mice spent more time approaching and in proximity to the novel object, *Arid1b*^{+/-} mice did not show any preference for exploring either familiar or novel objects (Fig. 6e). *Arid1b* conditional mutant mice (*Arid1b*^{loxP/+}; *Dlx5/6-Cre-IRES-EGFP*) showed similar impairments in recognition memory (Supplementary Fig. 13a). Additionally, the rotarod test revealed motor learning defects in *Arid1b*^{+/-} mice (Fig. 6f). These results demonstrate that *Arid1b*^{+/-} mice have impaired cognitive functioning in areas such as spatial and non-spatial learning and memory.

Next, we used the three-chamber social test to assess social interaction behavior. In the sociability test, control mice spent more time in the chamber containing an unfamiliar stranger mouse than in the empty chamber, whereas *Arid1b*^{+/-} and *Arid1b*^{loxP/+}; *DLX-Cre-IRES-EGFP* mice showed no preference for either chamber (Fig. 6g, Supplementary Fig. 13b). In a social novelty test, control mice showed preference for the second stranger mouse, whereas *Arid1b*^{+/-} and *Arid1b*^{loxP/+}; *DLX-Cre-IRES-EGFP* mice spent more time in the chamber containing the first, more familiar, stranger mouse. Social interaction in *Arid1b*^{+/-} mice was confirmed in an open-field apparatus. *Arid1b*^{+/-} mice exhibited reduced time spent with general sniffing, anogenital sniffing, and following behavior (Fig. 6h). Interestingly, approximately 20% of *Arid1b*^{+/-} mice demonstrated excessive grooming behavior, resulting in severe self-injury, such as torn ears or hair loss in face, neck, and shoulder regions (Fig. 6i, j). Excessive grooming was also observed in *Arid1b*^{loxP/+}; *Dlx5/6-Cre-IRES-EGFP*, and *Arid1b*^{loxP/+}; *Nkx2.1-Cre* mice (Supplementary Fig. 13c). These results show that *Arid1b*^{+/-} mice exhibit impaired social interaction and repetitive behaviors, which are core features of ASD.

Individuals with ASD frequently experience heightened anxiety. Using the elevated plus maze test and the open field test, we found that *Arid1b*^{+/-} and *Arid1b*^{loxP/+}; *DLX-Cre-IRES-EGFP* mice showed increased anxiety (Fig. 6k, l, Supplementary Fig. 13d, e). *Arid1b* mutant mice showed decreased moving distances in the open field test, compared with wild type mice (Supplementary Fig. 14a, b). We also performed the forced-swim test and the tail suspension test to assess depression-related behavior. *Arid1b*^{+/-} mice showed markedly increased immobilization behavior in both tests compared with control mice (Fig. 6m). Together, our behavioral assessment using *Arid1b*^{+/-} mice shows that *Arid1b* haploinsufficiency diminishes intellectual functioning and social interaction, and elevates anxiety-like behavior.

Because *Arid1b*^{+/-} mice showed a decreased number of GABAergic interneurons in the brain, we examined whether pharmacological modulation of GABA activity could rescue the abnormal behaviors observed in *Arid1b*^{+/-} mice. We first performed the novel object recognition test in control and *Arid1b*^{+/-} mice after intraperitoneal injection of clonazepam, a positive allosteric modulator of GABA_A receptor. Treatment with clonazepam increased the amount of time *Arid1b*^{+/-} mice spent investigating the novel object to wild type levels (Fig. 7a). In the three-chamber social test, clonazepam treatment did not induce changes in the measured sociability of either control or *Arid1b*^{+/-} mice (Fig. 7b). When a second stranger mouse was introduced for the social novelty assessment, however, clonazepam treatment of *Arid1b*^{+/-} mice successfully rescued the impaired social novelty phenotype. The clonazepam treatment also reversed the reduced center time and moving distance of *Arid1b* mutant mice in the open field test (Fig 7c, d, Supplementary Fig. 14c). However, depression measures using the forced swim test and the tail suspension test showed no reversible effect of clonazepam in *Arid1b*^{+/-} mice compared with controls (Fig. 7e, f). Our results showed that clonazepam rescues impaired recognition, social memory and elevated anxiety in *Arid1b*^{+/-} mice. The decreased mIPSC frequency in *Arid1b*^{+/-} cortical slices was also reversed by the clonazepam treatment (Supplementary Fig. 14d). The mIPSC amplitude was not changed in any condition. Full length Western blots are presented in Supplementary Fig. 15.

DISCUSSION

Despite recent advances in genetic studies of ASD and intellectual disability, the underlying mechanisms for these neurological conditions remain poorly understood. In this study, we showed that haploinsufficiency of the chromatin remodeling complex gene *Arid1b* disrupts normal interneuron development and function in the mouse brain. This is an important finding because, while *ARID1B* haploinsufficiency is known to cause ASD and intellectual disability^{2-4,20}, the cellular and molecular basis for *ARID1B* haploinsufficiency-related neurodevelopmental disorders has not been delineated. Our results suggest that *ARID1B* haploinsufficiency disrupts normal histone modifications and histone modifier access to some genes related to interneuron development. Another significant impact of this study is the creation of an animal model for *ARID1B* haploinsufficiency. The behavioral phenotypes of this mouse recapitulate the deficits in cognitive and social functions observed in individuals with ASD or intellectual disability. This mouse model can be further utilized for anatomical and functional studies examining abnormal neurodevelopmental conditions.

We found that cortical GABAergic interneurons were decreased in *Arid1b*^{+/-} and *Arid1b* conditional knockout mice, while interneuron migration routes and speeds remained normal. Thus, the depletion of interneurons in the cerebral cortex appears to be caused by defective proliferation and maintenance of interneuron progenitors in the MGE, the origin of as much as 60–80% of cortical interneurons²¹. This decrease in cortical interneurons in *Arid1b*^{+/-} and *Arid1b* conditional knockout mice was largely specific to parvalbumin-positive neurons. The number of calretinin-positive interneurons, which are mainly derived from the CGE, was not altered in *Arid1b*^{+/-} mice, suggesting that *ARID1B* haploinsufficiency may induce differential spatial sensitivity in progenitor regulation. Reduced inhibitory neurons may induce a compensatory increase in the number or level of inhibitory postsynaptic

components in *Arid1b* mutant brains. However, the levels of postsynaptic inhibitory components, *Gphn* and *Arhgef9*, were decreased in *Arid1b*^{+/-} cortices compared with control samples. Thus, in addition to the decreased inhibitory inputs, reduced reception capacity appears to contribute to the disrupted inhibitory transmission in *Arid1b*^{+/-} mice. Cortical excitatory neurons derived from radial progenitors showed grossly normal positioning, numbers and neurite morphology in *Arid1b*^{+/-} mice. Our previous work showed that *Arid1b* knockdown reduced dendritic arborization in cortical pyramidal neurons²². This study used shRNA to knockdown *Arid1b*. One of the limitations in shRNA-mediated gene knockdown is the difficulty in controlling the quantity of gene knockdown. More than half of *Arid1b* knockdown could alter pyramidal neuron morphology.

GABAergic interneurons play an important role as inhibitory neurons in neural circuitry by regulating pyramidal neuron activity. Alterations in parvalbumin interneuron numbers and *Pvalb* mRNA levels have been reported in autistic human brains²³⁻²⁸. Imbalanced E/I is associated with autistic brain composition and is generally caused by deficient GABAergic signaling, leading to broken circuit homeostasis^{8,29}. *Pvalb* knockout mice also show core symptoms of ASD and exhibit E/I imbalance^{30,31}. Consistently, our mouse model of ASD shows a selective reduction of parvalbumin-positive neurons as well as E/I imbalance in structural and functional synaptic connectivity. The decrease in GABAergic interneurons may cause imbalanced excitation and inhibition in *Arid1b*^{+/-} brains, leading to abnormal behavior similar to ASD. Aberrant neural mechanisms during interneuron development such as proliferation, placement, neurite outgrowth, and synapse formation might induce behavioral phenotypes individually or cooperatively in *Arid1b*^{+/-} mice. Specific aspects of interneuron development that play a key role in *Arid1b* haploinsufficiency-driven behavior remain to be elucidated. Also, we don't exclude the possibility that some impacts in excitatory neurons caused by *Arid1b* deficiency could have contributed to abnormal behavior in *Arid1b* mutant mice.

Our results demonstrated that the levels of histone acetylation and methylation were decreased in *Arid1b*^{+/-} mice, suggesting a role of ARID1B in remodeling the chromatin complex by inducing the physical access of histone modifying enzymes such as PCAF and CBP to histone molecules. As a result, the target genes in the condensed chromatin could be transformed into a more relaxed structure to create favorable environments for greater levels of gene transcription. The association of ARID1B with HATs or HDACs has been shown to regulate HAT and HDAC activity in mouse osteoblast cells³². However, we found no changes in activity of HATs or HDACs, or in the mRNA levels of multiple HAT, HDAC and histone genes in *Arid1b*^{+/-} cortices. These results suggest that ARID1B has no direct regulatory activity on HATs or HDACs in the brain. Rather, ARID1B may regulate histone modification via protein-protein interaction with histone modifiers. Recently, studies have shown that mutations in the gene encoding BRG1, the central subunit of the BAF chromatin remodeling complex, reduces the binding of the BAF complex to acetylated histones^{33,34}. The BAF complex is required for histone acetylation by acetyl transferase proteins³⁴. Our data showed that *Arid1b* haploinsufficiency decreases the expression levels of interneuron-associated genes, *Pvalb* and *Ntrk2*, and alters epigenetic signatures in the brain. Still, understanding the genomic mechanisms and parvalbumin neuron-specificity of these mechanisms requires further work. It is possible that the decreased number of parvalbumin-

positive neurons in *Arid1b* mutants could lead to the reduced epigenetic signatures for phospho-CTD (Ser5) and H3K9ac to the *Pvalb* promoter. Alternatively, given the high level changes in overall histone modifications in *Arid1b* mutant brains, the epigenetic changes may occur broadly in several other cell types.

Our mouse model effectively mirrors the behavioral characteristics of intellectual disability and ASD. *Arid1b*^{+/-} and *Arid1b* conditional knockout mice displayed impaired spatial learning, recognition memory, and reference memory. Open field and social behavior tests also revealed decreased social interaction in the mice. Mice with mutations in genes encoding *Smarca2* and *Actl6b*, other subunits of the BAF complex, have severe defects in social interaction and long-term memory³⁵. Thus, this chromatin remodeling complex may provide a cellular and molecular platform for normal intellectual and social behavior. In addition, *Arid1b*^{+/-} mice showed heightened levels of anxiety- and depression-related behaviors, which are common symptoms of ASD³⁶. For people with intellectual disability, the prevalence of anxiety disorders has likewise been shown to be much higher³⁷. This may be due to reduced cognitive function and increased vulnerability to environmental demands. Communication difficulties may also make it more difficult for people with cognitive disabilities to deal with anxiety or fear. ARID1B haploinsufficiency may be responsible for multiple facets of characteristic ASD behaviors. Other isoforms of *Arid1b* that are not affected by the *Arid1b* mutation could exist in the mouse line. Additionally, it is possible that the genetic background for the mouse line may impact the effect of *Arid1b* haploinsufficiency. Thus it is important to consider allele specificity, genetic backgrounds, and knockout strategies for comparing phenotypes of other *Arid1b* haploinsufficiency models. In a recent study, an *Arid1b* mouse generated using CRISPR/Cas9 gene-editing shows impairments in social and anxiety behavior as well as body growth³⁸. These phenotypes are consistent with our mouse model. However, the *Arid1b* mouse shows no learning, memory, and cognitive deficiencies, which is contrast with our findings and surprising given the association of *Arid1b* haploinsufficiency with intellectual disability.

GABA allosteric modulators including clonazepam, a benzodiazepine, have been used to treat seizures and anxiety³⁹. We found that clonazepam injection rescues deficits in object and social recognition and anxiety in *Arid1b*^{+/-} mice. These results suggest that treatment with a benzodiazepine could be a potential pharmacological intervention for symptoms of ASD. Furthermore, our results suggest that pharmacological manipulation of GABA signaling is a potential treatment strategy for cognitive and social dysfunctions in ASD- or intellectual disability-associated disorders due to mutations in chromatin remodeling genes.

METHODS

Methods, including statements of data availability and any associated accession codes and references, are available in the online version of the paper.

ONLINE METHODS

Generation of *Arid1b* knockout mice

The ES cell clone used for creating the *Arid1b* mouse model was the JM8.N4 strain obtained from the European Conditional Mouse Mutagenesis program (EUCOMM) and contains a “knockout first” design ([https://www.mousephenotype.org/data/alleles/MGI:1926129/tm1a\(EUCOMM\)Hmgu/](https://www.mousephenotype.org/data/alleles/MGI:1926129/tm1a(EUCOMM)Hmgu/) IKMC project ID: 25129). Exon 5 of the *Arid1b* gene was targeted to create a deletion allele. The knockout first allele for the *Arid1b* locus was created by injecting the targeted ES cell clones into the blastocysts derived from an albino C57BL6 strain (Jackson Laboratory, #000058) in the Mouse Genome Engineering Core Facility at the University of Nebraska Medical Center. The chimeras were first bred to a Flpo mouse strain (MMRRC UCD, stock # 036512) to delete the knockout first cassette in the intron 4–5 and convert the allele to the floxed allele. Elimination of the neomycin cassette was confirmed by PCR genotyping. The heterozygous floxed mice were crossed with appropriate Cre drivers for tissue-specific *Arid1b* deletion. To generate the global *Arid1b* KO allele, the knockout first allele was crossed with a CMV-Cre mouse strain (Jackson laboratory, #006054), and the resulting *Arid1b* KO allele in which the neo cassette, one FRT, one loxP, and exon 5 were removed was selected by genomic PCR and sequencing using appropriate primers. The genomic sequences showing the deletion break points of mutant genomic DNAs were shown in Supplementary Table 2. Based on the lack of protein in the null mice, we presume that the transcript from the deleted allele undergoes nonsense-mediated decay. The Mice were housed in a cage with 12:12h light-dark cycle. No more than 5 mice were housed in a cage. Mice were handled according to a protocol approved by the University Nebraska Medical Center Institutional Animal Care and Use Committee.

Real-time reverse transcription PCR

Quantitative real-time PCR was performed as described previously⁴⁰. Total RNA was extracted from wild-type and *Arid1b* mutant brain tissues using Trizol reagent (Invitrogen). First-strand complementary DNA (cDNA) was prepared by reverse transcription using the Verso cDNA synthesis kit (Thermo Fisher Scientific). To determine the conditions for the logarithmic phase during PCR amplification with target mRNA, aliquots (1 µg) were amplified using different numbers of cycles. A linear relationship between PCR product band visibility and number of amplification cycles was observed for target mRNAs. Real-time PCR was performed with 1 µl of the cDNA template added to 10 µl of 2x SYBR Premix Ex Taq (Applied Biosystems) and specific primers (10 pM each). Primer sequences are presented in Supplementary Table 3. Real-time PCR (Applied Biosystems) was carried out for 40 cycles of denaturation at 95°C for 15 sec, annealing at 58°C for 15 sec, and extension at 72°C for 15 sec. Target gene expression was quantified relative to that of an internal control gene (GAPDH) based on the comparison of the threshold cycle (CT) at constant fluorescence intensity. The amount of transcript was inversely related to the observed CT and the CT was expected to increase by 1 for every two-fold dilution of the transcript. Relative expression (R) was calculated using the equation $R = 2^{-[CT_{\text{sample}} - CT_{\text{control}}]}$. All data were normalized relative to GAPDH as well as to the respective controls.

Western blot analysis and Immunoprecipitation

Western blotting and immunoprecipitation were performed as described previously⁴¹. For Immunoprecipitation, rabbit-anti-H3K9ac antibody (Abcam, ab4441, 1:200), rabbit anti-CBP (Cell Signaling Technology, #7389, 1:200) and rabbit anti-PCAF (Cell Signaling Technology, #3378, 1:200) were immobilized on Dynabeads protein G (Invitrogen). Reaction mixtures were rocked at 4°C for 24 h and the beads were washed four times with washing buffer. The beads were separated from the supernatant by binding to DynaMag-2 (Life Technology). After running on a PAGE gel and performing membrane transfer, the resulting blot was subjected to Western blotting. Primary antibodies used for Western blotting were mouse anti-ARID1B (Abcam, ab57461, 1:1,000; Abnova, H00057492-M02, 1:1,000), mouse anti-GAD1 (Millipore, MAB5406, 1:1,000), rabbit anti-calbindin-D_{28k} (Millipore, AB1778, 1:1,000), mouse anti-calretinin (Millipore, MAB1568, 1:1,000), rabbit anti-H3K9ac (Abcam, ab4441, 1:1,500), rabbit anti-H3K4me3 (Cell Signaling Technology, #9751, 1:1,500), rabbit anti-H3K27me3 (Cell Signaling Technology, #9733, 1:1,500), rabbit anti-H3 (Cell Signaling Technology, #4499, 1:2,000), rabbit anti-Acetyl-CBP/p300 (Cell Signaling Technology, #4771, 1:800), rabbit anti-CBP (Cell Signaling Technology, #7389, 1:1,000), rabbit anti-PCAF (Cell Signaling Technology, #3378, 1:1,500), rabbit anti-HDAC4 (Sigma-Aldrich, H9411, 1:1,500), rabbit anti- β -catenin (Cell Signaling Technology, #8480, 1:1,000), rabbit anti-p- β -catenin (Phospho Solution, P120-3337, 1:1,000), rabbit anti-Cyclin D1 (Cell Signaling Technology, #2922, 1:1,000), rabbit anti-HA (Cell Signaling Technology, #3724, 1:1,500) or rabbit anti-GAPDH (Millipore, MAB374, 1:2,000). Membranes were developed and imaged using ECL chemiluminescence reagent (Thermo Fisher Scientific) and the Fluo-chem HD2 imaging system (ProteinSimple), respectively. Signal specificity was ensured by omitting each primary antibody. For quantification of band intensity, blots from 3 independent experiments for each molecule of interest were analyzed using ImageJ software (NIH). Background samples from an area near each lane were subtracted from each band to acquire mean band density. GAPDH was used as an internal control to normalize band intensity.

Immunostaining

Immunostaining of brain sections or dissociated cells was performed as described previously^{42,43}. Primary antibodies used were mouse anti-ARID1B (Abcam, ab57461, 1:500; Abnova, H00057492-M02, 1:500), rabbit anti-GABA (Sigma, A2052, 1:500), mouse anti-parvalbumin (Millipore, MAB1572, 1:500), rabbit anti-cleaved caspase-3 (Cell Signaling Technology, #9664, 1:300), mouse anti-BrdU (BD Biosciences, #555627, 1:800), rabbit anti-Phospho-Histone H3 (Cell Signaling Technology, #9701, 1:800), rabbit anti-VIAAT (Phosphosolution, 2100-VGAT, 1:500), guinea pig anti-VGluT11 (Millipore, AB5905, 1:500), rat anti-GAD2 (Developmental Studies Hybridoma Bank, GAD6, 1:500), rat anti-somatostatin (Millipore, MAB354, 1:500), rabbit anti-calbindin-D_{28k} (Millipore, AB1778, 1:500), mouse anti-calretinin (Millipore, MAB1568, 1:500), rabbit anti-Cux1 (Santa Cruz, sc-13024, 1:500), mouse anti-NeuN (Millipore, MAB377, 1:1000), rabbit anti-TBR1 (Millipore, AB10554, 1:500), rabbit anti-Olig2 (Millipore, AB9610, 1:500), rabbit anti-GFAP (DAKO, Z0334, 1:500), rabbit anti-PSD95 (Abcam, ab18258, 1:500) and chicken anti-GFP (Invitrogen, A10262, 1:1,500) antibodies. Appropriate secondary

antibodies conjugated with Alexa dyes (Invitrogen) were used to detect primary antibodies. DAPI (Sigma-Aldrich) was used to stain nuclei.

Morphometry

For the quantification of numbers and lengths of cells and neurites, images of 20 different brain sections at periodic distances along the rostro-caudal axis were taken with Zeiss LSM710 confocal microscopes as described previously⁴⁴. N numbers for each experiment were described in figure legends. Mouse Cultured neurons were also assessed with these microscopes. More than 20 fields scanned horizontally and vertically were examined in each condition. Cell numbers were described in figure legends. The images were analyzed using ZEN (Zeiss), QCapture software (QImaging), and ImageJ (NIH). The calculated values were averaged, and some results were recalculated as relative changes versus control.

Cell culture

The medial ganglionic eminence (MGE) cells were isolated from E12.5–14.5 mice. Meninges were removed and MGE cells were dissociated with trituration after trypsin/EDTA treatment. The cells were plated onto poly-D-lysine/laminin-coated coverslips and cultured in the medium containing Neurobasal medium (Invitrogen), 2 mM glutamine, 2% (v/v) B27 supplement (Invitrogen), 1% (v/v) N2 supplement (Invitrogen), and 50 U/mL penicillin/streptomycin (Invitrogen).

TUNEL assay

As described previously⁴⁵, tissue sections and cell cultures were fixed with 4% PFA, and in situ detection of cells with DNA-strand breaks was performed using In Situ Cell Death Detection Kit (Roche Diagnostics) according to the manufacture's instruction.

Time-lapse experiments

Organotypic brain slices were prepared from E13.5 mice as described previously^{46,47}. Cortical slices from *Dlx5/6-Cre-IRES-EGFP* mice crossed with *Arid1b^{+/+}* or *Arid1b^{+/-}* allele were embedded in 3% low melting point agarose and coronal cortical slices at 250 μ m thickness were prepared using a LEICA VT1000S vibratome. The slices were then placed on poly-lysine/laminin-coated transwell inserts and cultured in neurobasal media organotypically using an air interface protocol until imaging. For time-lapse imaging, an LSM710 inverted confocal microscope (Zeiss) equipped with a CO₂ incubator chamber (5% CO₂, 37°C) was used. Multiple Z-stacks with the options of 10–20 successive 'z' optical planes spanning 50–70 μ m were acquired on pre-selected positions of electroporated slices. Repetitive imaging was performed every 30 min for up to 8 h. Mean velocity of migrating cells was obtained using the ImageJ plug-in Manual Tracking.

Electron microscopy

Brains were fixed in 2% glutaraldehyde and 2% paraformaldehyde in 0.1 M cacodylate buffer overnight at 4°C. Coronal brain slices (150 μ m) were made with a vibratome. Samples were then post-fixed with 1% OsO₄ for 1 h, dehydrated, and embedded in Araldite resin (Electron Microscopy Sciences). Thin sections (60 nm) were post-stained with 2%

uranyl acetate and Reynold's lead citrate. Imaging was performed on a FEI Tecnai G2 Spirit transmission electron microscope equipped with a LAB6 crystal operating at an accelerating voltage of 80 kV. The digital images were captured with AMT CCD camera. Excitatory and inhibitory synapses were analyzed separately after classification into "symmetric" and "asymmetric" synapses. The synaptic cleft was measured as the gap between the presynaptic and postsynaptic membranes in digitally magnified images. The synaptic length was assessed as the length of postsynaptic density.

Whole-cell electrophysiology and data analysis

Voltage-clamp whole-cell recordings were obtained from slices of wild-type and mutant cerebral cortices. Acute prefrontal cortical slices were placed in ice-cold artificial cerebrospinal fluid (ACSF) of the following composition (in mM): 130 NaCl, 24 NaHCO₃, 3.5 KCl, 1.25 NaH₂PO₄, 2.4 CaCl₂, 2.5 MgCl₂ and 10 glucose saturated with 95% O₂/5% CO₂. 300 μm thick coronal sections were collected using vibrating microtome (Leica VT1200, Buffalo Grove, IL, USA). Whole-cell patch recordings were obtained from layer V prelimbic cortical pyramidal neurons with patch pipettes (3–5 mOhm) filled with a solution containing 126 mM cesium methanesulfonate, 8 mM NaCl, 10 mM HEPES, 2.9 mM QX-314, 8 mM Na₂-phosphocreatine, 0.3 mM Na₂GTP, 4 mM MgATP, 0.1 mM CaCl₂, 1 mM EGTA (pH 7.3). Neurons were held at a holding potential of –70 mV for mEPSCs and 0 mV for mIPSCs. For recording mEPSCs 1 μM tetrodotoxin and 100 μM picrotoxin were added to the external recording solution, and for mIPSCs 1 μM tetrodotoxin, 10 μM NBQX and 50 μM D-AP5 were added. The slices were treated with 10 μM clonazepam for 7 min after 5 min baseline recording and followed by 7 min wash. Signal was filtered at 2 kHz and digitized at 20 kHz using an Axon Digidata 1440A analog-to-digital board (Molecular Devices). Recordings were performed from three mice for each genotype. Recordings with a pipette access resistance less than 20 mOhm and that of less than 20% changes during the duration of recording were included. The mEPSC and mIPSC recordings were analyzed using minianalysis software (Synapsoft) with an amplitude threshold set at 6–8 pA for cultured neuron recordings and 5 pA for slice recordings. The frequency, amplitude and decay were measured in each group.

Chromatin Immunoprecipitation (ChIP) PCR assay

ChIP analysis was performed by using the Magna ChIP Kit (Millipore). Briefly, *Arid1b* mutant cortical tissues were cross-linked with 1.5% formaldehyde for 20 min at room temperature. This reaction was stopped by adding 0.125 M glycine for 5 min, and the samples were then washed three times with PBS at room temperature. Tissues were dissociated with 20–25 strokes by the Dounce Homogenizer (Wheaton). Dissociated cells were then lysed and sonicated with the S220 High Performance Ultrasonicator (Covaris). Sonicated chromatin, dynabeads protein A/G (Invitrogen) and appropriate antibodies were mixed and incubated overnight at 4°C with gentle shaking. ChIP-grade anti-H3K9ac (Abcam, ab4441, 1:100), anti-ARID1B (Abcam, ab57461, 1:100) and anti-RNA polymerase II phospho-Ser5 (Abcam, ab5131, 1:100) antibodies were used. Beads were washed and reverse cross-linked according to the Magna ChIP Kit protocol. The DNA captured by the immunoprecipitated protein was subjected to PCR.

BioID pull down

The *Histone H3 (H3)* cDNA was amplified by PCR and inserted into the MCS-BioID2-HA vector (Addgene) using *EcoRI* and *BamHI* sites. Proximity-dependent biotin identification (BioID) pull down was performed as described previously¹⁶. The cloned *H3* in MCS-BioID2-HA vector was transfected into MGE cells using Lipofectamine LTX (Life Technology), as recommended by the manufacturer. At 6 days in vitro (DIV) MGE cells were incubated with 50 μ M biotin for 18 hours. After two PBS washes, cells were lysed in lysis buffer containing 50 mM Tris, pH 7.4, 500 mM NaCl, 0.4% SDS, 1 mM dithiothreitol, and 1 \times protease inhibitor (Thermo Fisher Scientific). Cells were collected and treated with Triton X-100 to a 2% final concentration. After two 1 minute rounds of sonication each at 30% duty cycle and an output level of 4 (Sonifier-250; Branson), an equal volume of 50 mM Tris, pH 7.4, was added and cleaned using centrifugation at 16,500 \times g for 10 min. The supernatant was collected in a 15-ml conical tube and incubated with 300 μ l Dynabeads overnight. Beads were collected using a magnetic stand and washed twice with 2% (wt/vol) SDS, once with wash buffer containing 0.1% deoxycholate, 1% Triton X-100, 500 mM NaCl, 1 mM EDTA, and 50 mM 4-(2-hydroxyethyl)-1-piperazineethanesulfonic acid, pH 7.5, once with wash buffer containing 250 mM LiCl, 0.5% NP-40, 0.5% deoxycholate, 1 mM EDTA, and 10 mM Tris, pH 8, and once with 50 mM Tris.

Golgi staining

Golgi staining was performed using the FD Rapid Golgi Stain kit (FD NeuroTechnologies). Freshly dissected brains were immersed in solutions A and B for 2 weeks at room temperature and then transferred into solution C for 24 h at 4°C in the dark. The brains were sliced using a vibratome (Leica) at a thickness of 80 μ m.

Behavioral assays

All behavioral assays were done during light cycle. Health conditions including weights, activity and feeding were checked prior to assays. We used 3–4 month-old male and female mice for most behavioral assays. For social behavior assays, we used only male mice because sexual interactions between males and females may interfere with accurate interpretation of social behavior. All behavioral assays were done blind to genotypes with age-matched littermates of mice.

Morris water maze test—Mice were introduced into the perimeter of a circular water-filled tank 110 cm in diameter and 91 cm in height (San Diego Instruments) with visual cues that were present on the tank walls as spatial references. The tank was divided into four equal quadrants (Q1–4) by lines drawn on the floor. A 10 cm circular plexiglass platform was submerged 1 cm deep in Q2 and as such hidden from the mice. The mice started the task from one of three quadrants Q1, Q3 and Q4, varied by day of testing. Four trials were performed per mouse per day for ten days. Each trial lasted 1 minute and ended when the mouse climbed onto and remained on the hidden platform for ten seconds. The mouse was given 20 seconds to rest on the platform between trials. The time taken by the mouse to reach the platform was recorded as its latency. The time for four trials was averaged and recorded as a result for each mouse. On day 11, the mice were subjected to a single 60-

second probe trial without a platform to test memory retention. The mice started the trial from Q4, number of annulus crossings was counted, and the swimming path was recorded and analyzed using the Ethovision XT 7 tracking software (Noldus).

T-Maze test—A mouse was first subjected to food-deprivation to 85% of their free-feeding body weight before starting the appetitively-motivated T-maze test. The T-Maze apparatus contained the start arm (28 wide × 5 long × 10 high cm) and the two identical goal arms (35 × 5 × 10 cm) surrounded by a 10 cm high wall. The test mouse was habituated to the T-maze apparatus and allowed to obtain food from the end of goal arms for 5 mins. Ten training trials per day were then performed for 5 days. One reinforcer (Noyes sucrose pellet, 20 mg) was available in the designated goal arm for each trial. At the beginning of each test session, the mouse was placed in the start box at the bottom of the start arm. When the start box door was opened, the mouse was given a choice between entering either goal arm. If the mouse made the correct choice, it was given time to consume the sugar pellet, and then guided back into the start box for the next trial. Incorrect choices were not rewarded. For each successive trial, the reward was always placed in the same arm.

Novel object recognition test—A test mouse was first habituated to an open field arena (35 × 42 cm) for 5 min. Following habituation, the test mouse was removed from the arena and two identical objects with size (10.5 × 4.5 × 2.5 cm) were placed in the opposite corners of the arena, 7 cm from the side walls. Then the test mouse was reintroduced into the center of the arena and allowed to explore the arena including the two novel objects for 10 min. After 6 h, one object was replaced with another novel object, which was of similar size but different shape and color than the previous object. The same test mouse was placed in the arena to explore the arena and the two objects. The movement of mice was recorded by a camera for 10 min and further analyzed by the video tracking EthoVision XT 7 software (Noldus).

Rotarod test—Using an accelerating Rotamex 4/8 (Columbus Instruments International) the rotarod test was performed by placing mice on rotating drums (3 cm diameter) and measuring retention time on the rod. The speed of the rotarod accelerated from 4 to 40 rpm over a 5-min period. Three trials per day over a 16-day period were conducted. At least 20 min recovery time was allowed between trials.

Three-chamber test for social interaction and novelty behavior—Social behavior was evaluated as described previously⁴⁰. A rectangular and transparent Plexiglas box divided by walls into three equal-sized compartments (Ugobasile) was used. Rectangular holes in the Plexiglas walls provide access between the chambers. For sociability testing, the test mouse was moved to the center chamber (chamber 2) with the entrances to the two connecting chambers blocked. A stimulus mouse (unfamiliar mouse) designated as “stranger 1” was placed in a wire enclosure in chamber 1. Then, the openings to the flanking two chambers (1 and 3) were opened and the test mouse was allowed to explore the entire apparatus for 10 min. For the social novelty test, the stranger 1 mouse was randomly placed in one of the enclosures in which the test mouse had the choice of whether to investigate the stranger 1 mouse or a novel mouse, designated “stranger 2”. This novel mouse was taken

from a different home cage and placed into the remaining empty wire enclosure. Time spent sniffing each partner by the test mouse was recorded for 10 min in both sociability and social novelty behavior tests. All apparatus chambers were cleaned with water and dried with paper towels between trials. At the end of each test day, the apparatus was sprayed with 70% ethanol and wiped clean with paper towels.

Open field social interaction test—Two *Arid1b* mutant or wild-type mice were placed in opposite corners of the open-field arena and allowed to explore freely for 10 min. Frequency and total duration of the active socio-positive behaviors including general sniffing, anogenital sniffing, following, mounting, and fighting were scored.

Spontaneous self-grooming—A mouse was placed in a clear plastic cage (17 × 32 × 14 cm). The mouse was allowed to freely explore the cage for the entirety of the test. The first 10 min served as a habituation period. The movement of the mouse was recorded by a camera for 30 min. Recorded grooming behaviors included head washing, body grooming, genital/tail grooming and paw and leg licking.

Elevated plus-maze test—The elevated plus-maze test was performed as previously described⁴⁰. The apparatus (EB Instrument) includes two open arms (35 × 5 cm), two enclosed arms (35 × 5 × 15 cm), and a central platform (5 × 5 cm). The entire apparatus was elevated 45 cm above the floor. A mouse was placed on the central platform, facing the same open arm and allowed to roam freely for 5 minutes. The number of entries into, and the time spent on open and closed arms were recorded. Percent open arm time was calculated as time spent in the open arms divided by the total time. Rearing frequency was also recorded.

Open field test—A mouse was placed near the wall-side of a 35 × 42 cm open-field arena, and the movement of the mouse was recorded by a camera for 5 min. The recorded video file was further analyzed using EthoVision XT 7.0 software (Noldus). The number of entries into, and the overall time spent in, the center of the arena (15 × 15 cm imaginary square) were measured. The open field arena was cleaned with 70% ethanol between each trial.

Forced swimming test—A mouse was placed individually into a glass cylinder (20 cm height, 17 cm diameter) filled with water to a depth of 10 cm at 25°C. After 5 minutes, the animals were removed from the water, dried, and returned to their home cages. They were again placed in the cylinder 24 hr later, and after the initial 1 min acclimatization period, the total duration of immobility was measured for 5 min. Motionless floating was considered immobile behavior.

Tail suspension test—A mouse was suspended from the hook of a tail suspension test box, 60 cm above the surface of a table using adhesive tape placed 1 cm away from the tip of the tail. After 1 min acclimatization, immobility duration was recorded by a camera for 5 minutes. Mice were considered immobile only when they hung passively and were completely motionless.

Statistical analysis

Normal distribution was tested using Kolmogorov-Smirnov test and variance was compared. Unless otherwise stated, statistical significance was determined using two-tailed unpaired Student's t-tests for two population comparison or one-way ANOVA followed by the Bonferroni's post hoc test for multiple comparisons. Data were analyzed using the GraphPad Prism and presented as means \pm SEM. P values for each comparison were described in the results, legends, or supplementary information section. To determine and confirm sample sizes (N), we performed a power analysis. The values for the power ($1-\beta$) and the type I error rate (α) were 0.8 and 0.05 (or 0.01), respectively. Each experiment in this study was performed blind and randomized. Animals were assigned randomly to the various experimental groups, and data were collected and processed randomly. The allocation, treatment, and handling of animals were the same across study groups. Control animals were selected from the same litter as the test group. The individuals conducting the experiments were blinded to group allocation and the allocation sequence. Exclusion criteria for mice were based on abnormal health conditions including weights below 15g at 6 weeks and noticeably reduced activity or feeding. Statistical data and N numbers for all behavioral assays were described in Supplementary Table 4.

Supplementary Material

Refer to Web version on PubMed Central for supplementary material.

Acknowledgments

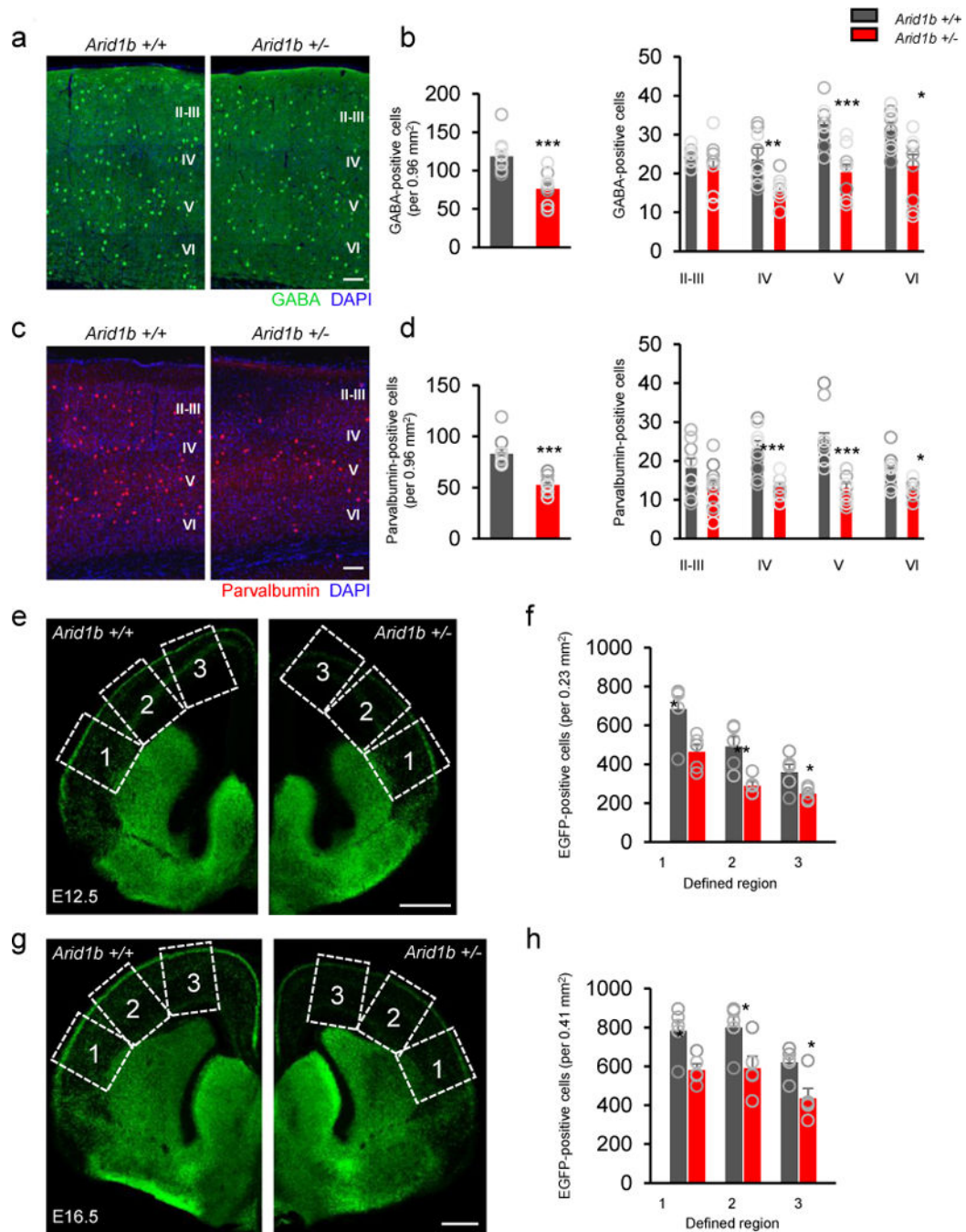
Research reported in this publication was supported by an award from the National Institute of Neurological Disorders and Stroke of the National Institutes of Health under award number R01NS091220 and an Institutional Development Award (IDeA) from the National Institute of General Medical Sciences of the National Institutes of Health under award number P20GM103471 to WYK.

References

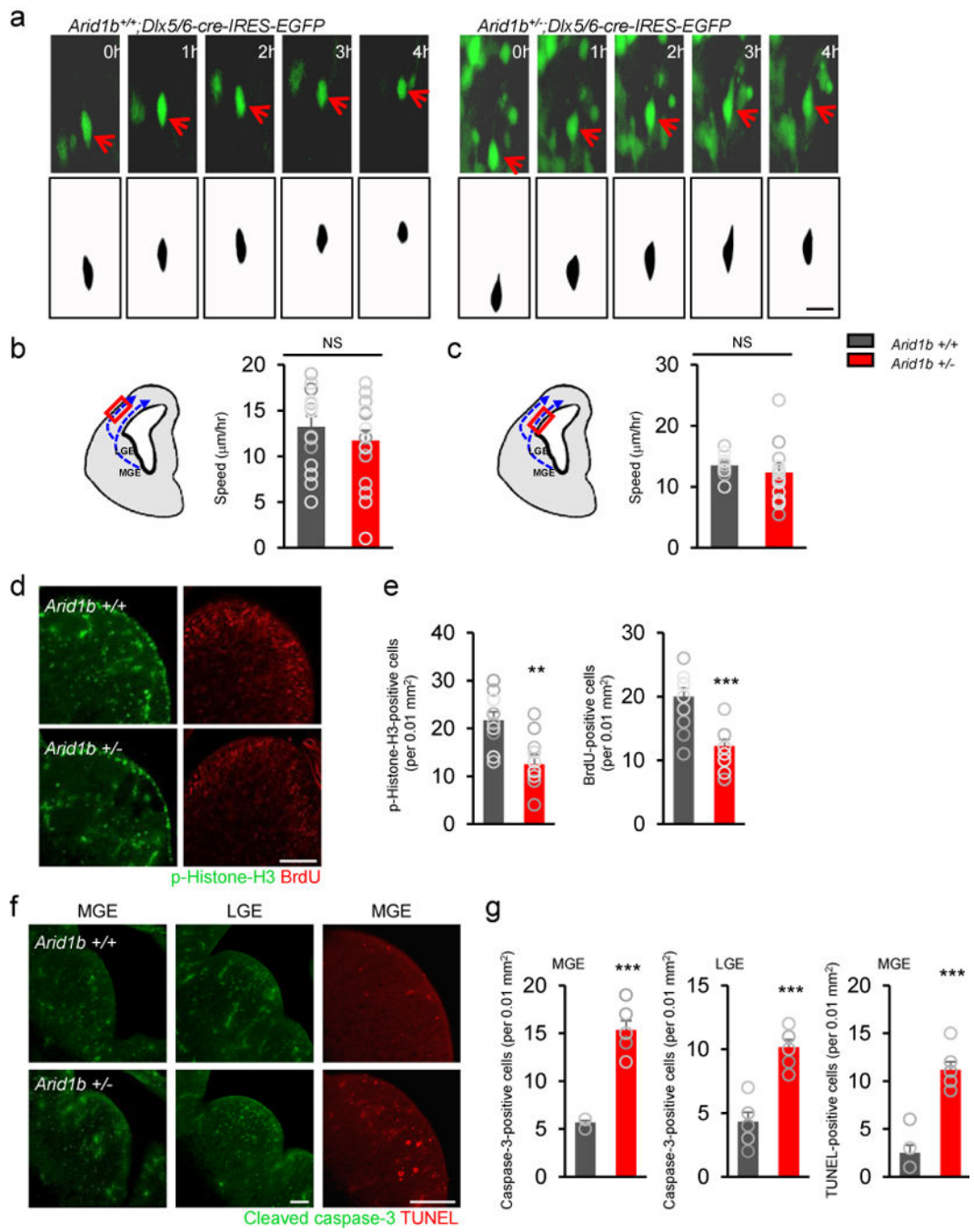
1. Ellison JW, Rosenfeld JA, Shaffer LG. Genetic basis of intellectual disability. *Annu Rev Med.* 2013; 64:441–450. [PubMed: 23020879]
2. Halgren C, et al. Corpus callosum abnormalities, intellectual disability, speech impairment, and autism in patients with haploinsufficiency of ARID1B. *Clin Genet.* 2012; 82:248–255. [PubMed: 21801163]
3. Santen GW, et al. Mutations in SWI/SNF chromatin remodeling complex gene ARID1B cause Coffin-Siris syndrome. *Nat Genet.* 2012; 44:379–380. [PubMed: 22426309]
4. Hoyer J, et al. Haploinsufficiency of ARID1B, a member of the SWI/SNF-a chromatin-remodeling complex, is a frequent cause of intellectual disability. *Am J Hum Genet.* 2012; 90:565–572. [PubMed: 22405089]
5. Ronan JL, Wu W, Crabtree GR. From neural development to cognition: unexpected roles for chromatin. *Nat Rev Genet.* 2013; 14:347–359. [PubMed: 23568486]
6. Lopez AJ, Wood MA. Role of nucleosome remodeling in neurodevelopmental and intellectual disability disorders. *Front Behav Neurosci.* 2015; 9:100. [PubMed: 25954173]
7. Marin O. Interneuron dysfunction in psychiatric disorders. *Nat Rev Neurosci.* 2012; 13:107–120. [PubMed: 22251963]
8. Nelson SB, Valakh V. Excitatory/Inhibitory Balance and Circuit Homeostasis in Autism Spectrum Disorders. *Neuron.* 2015; 87:684–698. [PubMed: 26291155]

9. Ben-Ari Y. The GABA excitatory/inhibitory developmental sequence: a personal journey. *Neuroscience*. 2014; 279:187–219. [PubMed: 25168736]
10. Robertson CE, Ratai EM, Kanwisher N. Reduced GABAergic Action in the Autistic Brain. *Curr Biol*. 2015; 26:80–85. [PubMed: 26711497]
11. Han S, et al. Autistic-like behaviour in *Scn1a*^{+/-} mice and rescue by enhanced GABA-mediated neurotransmission. *Nature*. 2012; 489:385–390. [PubMed: 22914087]
12. Moffat JJ, Ka M, Jung EM, Kim WY. Genes and brain malformations associated with abnormal neuron positioning. *Mol Brain*. 2015; 8:72. [PubMed: 26541977]
13. Skarnes WC, et al. A conditional knockout resource for the genome-wide study of mouse gene function. *Nature*. 2011; 474:337–342. [PubMed: 21677750]
14. Stenman J, Toresson H, Campbell K. Identification of two distinct progenitor populations in the lateral ganglionic eminence: implications for striatal and olfactory bulb neurogenesis. *The Journal of neuroscience: the official journal of the Society for Neuroscience*. 2003; 23:167–174. [PubMed: 12514213]
15. Xu Q, Tam M, Anderson SA. Fate mapping *Nkx2.1*-lineage cells in the mouse telencephalon. *The Journal of comparative neurology*. 2008; 506:16–29. [PubMed: 17990269]
16. Kim DI, et al. An improved smaller biotin ligase for BioID proximity labeling. *Mol Biol Cell*. 2016; 27:1188–1196. [PubMed: 26912792]
17. Sommeijer JP, Levelt CN. Synaptotagmin-2 is a reliable marker for parvalbumin positive inhibitory boutons in the mouse visual cortex. *PloS one*. 2012; 7:e35323. [PubMed: 22539967]
18. Lucas EK, et al. PGC-1 α provides a transcriptional framework for synchronous neurotransmitter release from parvalbumin-positive interneurons. *The Journal of neuroscience: the official journal of the Society for Neuroscience*. 2014; 34:14375–14387. [PubMed: 25339750]
19. Cowell RM, Blake KR, Russell JW. Localization of the transcriptional coactivator PGC-1 α to GABAergic neurons during maturation of the rat brain. *The Journal of comparative neurology*. 2007; 502:1–18. [PubMed: 17335037]
20. Tsurusaki Y, et al. Mutations affecting components of the SWI/SNF complex cause Coffin-Siris syndrome. *Nat Genet*. 2012; 44:376–378. [PubMed: 22426308]
21. Wonders CP, Anderson SA. The origin and specification of cortical interneurons. *Nat Rev Neurosci*. 2006; 7:687–696. [PubMed: 16883309]
22. Ka M, Chopra DA, Dravid SM, Kim WY. Essential Roles for ARID1B in Dendritic Arborization and Spine Morphology of Developing Pyramidal Neurons. *The Journal of neuroscience: the official journal of the Society for Neuroscience*. 2016; 36:2723–2742. [PubMed: 26937011]
23. Zikopoulos B, Barbas H. Altered neural connectivity in excitatory and inhibitory cortical circuits in autism. *Front Hum Neurosci*. 2013; 7:609. [PubMed: 24098278]
24. Stoner R, et al. Patches of disorganization in the neocortex of children with autism. *N Engl J Med*. 2014; 370:1209–1219. [PubMed: 24670167]
25. Reynolds GP, Zhang ZJ, Beasley CL. Neurochemical correlates of cortical GABAergic deficits in schizophrenia: selective losses of calcium binding protein immunoreactivity. *Brain Res Bull*. 2001; 55:579–584. [PubMed: 11576754]
26. Lawrence YA, Kemper TL, Bauman ML, Blatt GJ. Parvalbumin-, calbindin-, and calretinin-immunoreactive hippocampal interneuron density in autism. *Acta Neurol Scand*. 2010; 121:99–108. [PubMed: 19719810]
27. Mariani J, et al. FOXP1-Dependent Dysregulation of GABA/Glutamate Neuron Differentiation in Autism Spectrum Disorders. *Cell*. 2015; 162:375–390. [PubMed: 26186191]
28. Gogolla N, et al. Common circuit defect of excitatory-inhibitory balance in mouse models of autism. *J Neurodev Disord*. 2009; 1:172–181. [PubMed: 20664807]
29. Cellot G, Cherubini E. GABAergic signaling as therapeutic target for autism spectrum disorders. *Front Pediatr*. 2014; 2:70. [PubMed: 25072038]
30. Wöhr M, et al. Lack of parvalbumin in mice leads to behavioral deficits relevant to all human autism core symptoms and related neural morphofunctional abnormalities. *Transl Psychiatry*. 2015; 5:e525. [PubMed: 25756808]

31. Saunders JA, et al. Knockout of NMDA receptors in parvalbumin interneurons recreates autism-like phenotypes. *Autism Res.* 2013; 6:69–77. [PubMed: 23441094]
32. Nagl NG Jr, Wang X, Patsialou A, Van Scoy M, Moran E. Distinct mammalian SWI/SNF chromatin remodeling complexes with opposing roles in cell-cycle control. *EMBO J.* 2007; 26:752–763. [PubMed: 17255939]
33. Chatterjee N, et al. Histone H3 tail acetylation modulates ATP-dependent remodeling through multiple mechanisms. *Nucleic Acids Res.* 2011; 39:8378–8391. [PubMed: 21749977]
34. Naidu SR, Love IM, Imbalzano AN, Grossman SR, Androphy EJ. The SWI/SNF chromatin remodeling subunit BRG1 is a critical regulator of p53 necessary for proliferation of malignant cells. *Oncogene.* 2009; 28:2492–2501. [PubMed: 19448667]
35. Vogel-Ciernia A, et al. The neuron-specific chromatin regulatory subunit BAF53b is necessary for synaptic plasticity and memory. *Nat Neurosci.* 2013; 16:552–561. [PubMed: 23525042]
36. Boyd K, Woodbury-Smith M, Szatmari P. Managing anxiety and depressive symptoms in adults with autism-spectrum disorders. *J Psychiatry Neurosci.* 2011; 36:E35–36. [PubMed: 21693092]
37. Reid KA, Smiley E, Cooper SA. Prevalence and associations of anxiety disorders in adults with intellectual disabilities. *J Intellect Disabil Res.* 2011; 55:172–181. [PubMed: 21205039]
38. Celen C, et al. *Arid1b* haploinsufficient mice reveal neuropsychiatric phenotypes and reversible causes of growth impairment. *eLife.* 2017; 6
39. Dahlin MG, Amark PE, Nergardh AR. Reduction of seizures with low-dose clonazepam in children with epilepsy. *Pediatr Neurol.* 2003; 28:48–52. [PubMed: 12657420]
40. Jung EM, Ka M, Kim WY. Loss of GSK-3 Causes Abnormal Astrogenesis and Behavior in Mice. *Molecular neurobiology.* 2016
41. Ka M, Kim WY. Microtubule-Actin Crosslinking Factor 1 Is Required for Dendritic Arborization and Axon Outgrowth in the Developing Brain. *Molecular neurobiology.* 2016; 53:6018–6032. [PubMed: 26526844]
42. Ka M, Kook YH, Liao K, Buch S, Kim WY. Transactivation of TrkB by Sigma-1 receptor mediates cocaine-induced changes in dendritic spine density and morphology in hippocampal and cortical neurons. *Cell death & disease.* 2016; 7:e2414. [PubMed: 27735948]
43. Ka M, Smith AL, Kim WY. mTOR controls genesis and autophagy of GABAergic interneurons during brain development. *Autophagy.* 2017; 13:1348–1363. [PubMed: 28598226]
44. Ka M, Condorelli G, Woodgett JR, Kim WY. mTOR regulates brain morphogenesis by mediating GSK3 signaling. *Development.* 2014; 141:4076–4086. [PubMed: 25273085]
45. Jung EM, An BS, Choi KC, Jeung EB. Apoptosis- and endoplasmic reticulum stress-related genes were regulated by estrogen and progesterone in the uteri of calbindin-D(9k) and -D(28k) knockout mice. *J Cell Biochem.* 2011; 113:194–203.
46. Ka M, Jung EM, Mueller U, Kim WY. MACF1 regulates the migration of pyramidal neurons via microtubule dynamics and GSK-3 signaling. *Dev Biol.* 2014; 395:4–18. [PubMed: 25224226]
47. Ka M, Moffat JJ, Kim WY. MACF1 Controls Migration and Positioning of Cortical GABAergic Interneurons in Mice. *Cerebral cortex.* 2016



4.794, *** $P=0.0001$; GABA layer VI: $t_{18}=3.024$, ** $P=0.0073$; parvalbumin layer IV: $t_{18}=4.515$, *** $P=0.0003$; parvalbumin layer V: $t_{18}=4.386$, *** $P=0.0004$; parvalbumin layer VI: $t_{18}=2.496$, * $P=0.0225$). $N=10$ mice for *Arid1b*^{+/+} (8 males, 2 females) and *Arid1b*^{+/-} (7 males, 3 females). Statistical significance was determined by a two-tailed Student's *t* test. **(e-h)** Interneurons expressing EGFP were assessed in E12.5 **(e)** and E16.5 **(g)** cortices from *Arid1b*^{+/+}; *Dlx5/6-Cre-IRES-EGFP* and *Arid1b*^{+/-}; *Dlx5/6-Cre-IRES-EGFP* mice. Scale bar= 400 μm . **(f and h)** Quantified numbers of cortical interneurons shown in **e** (region 1: $t_8=2.849$, * $P=0.0215$; region 2: $t_8=3.664$, ** $P=0.0064$; region 3: $t_8=2.495$, * $P=0.0372$) and **g** (region 1: $t_8=3.112$, * $P=0.0144$; region 2: $t_8=2.545$, * $P=0.0344$; region 3: $t_8=3.044$, * $P=0.016$). The cortex was divided into three equally defined regions along the lateral cortex as indicated by dashed boxes and numbers. $N=5$ mice for each age and group. Statistical significance was determined by a two-tailed Student's *t* test. Data shown are the mean \pm SEM.



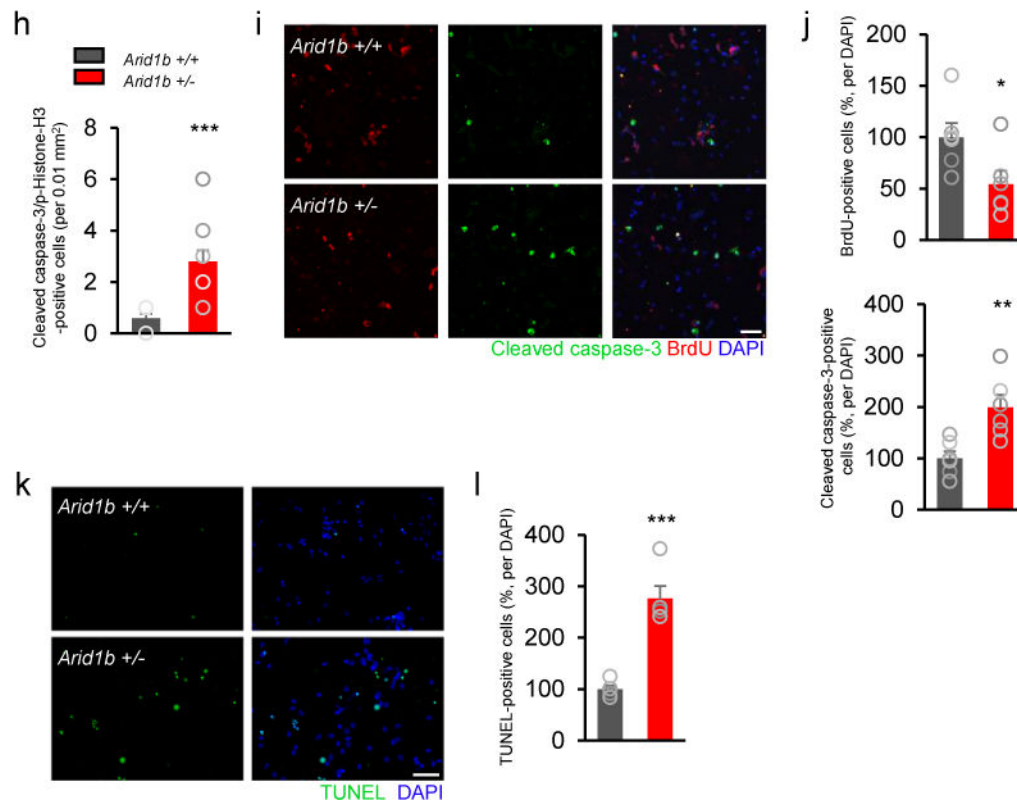


Figure 2. Migration, apoptosis, and proliferation of interneuron progenitors in *Arid1b*^{+/-} mice (a) Using time-lapse imaging, interneuron migration was assessed in organotypic slices from E13.5 *Arid1b*^{+/+};*Dlx5/6-Cre-IRES-EGFP* and *Arid1b*^{+/-};*Dlx5/6-Cre-IRES-EGFP* cortices. The speed of interneuron migration was not different between EGFP-positive neurons from *Arid1b*^{+/+};*Dlx5/6-Cre-IRES-EGFP* and *Arid1b*^{+/-};*Dlx5/6-Cre-IRES-EGFP* cortices. Red arrows indicate the same cell traced by time-lapse imaging. Scale bar= 30 μ m. (b and c) Interneuron migration speed was measured along two known interneuron migratory routes; one along the marginal zone (b) and the other along the ventral zone (c). N= 20 cells from 3 mice for each condition. Statistical significance was determined by a two-tailed Student's *t* test. NS: no significance. (d) *Arid1b* haploinsufficiency decreases progenitor proliferation in the MGE. Ventral brain sections containing *Arid1b*^{+/+} and *Arid1b*^{+/-} MGEs at E12.5 were immunostained with phospho-histone H3 and BrdU antibodies after a 24 h BrdU pulse. (e) Quantification of d. Histograms show the numbers of phospho-histone H3 (t_{18} = 3.487, ***P*= 0.0026) and BrdU (t_{22} = 4.704, ****P*= 0.0001)-positive cells per 0.01 mm² in the MGE. Scale bar= 100 μ m. N= 10 mice for each group for phospho-histone H3, and 12 mice for each group for BrdU. Statistical significance was determined by a two-tailed Student's *t* test. (f) Cell death was assessed in control and mutant MGEs and LGEs by immunostaining using a cleaved caspase-3 antibody or by the TUNEL assay. (g) Quantification of f. Mutant GEs had more dying cells. N= 6 mice for each group. Statistical significance was determined by a two-tailed Student's *t* test. Cleaved caspase-3 (MGE: t_{10} = 6.246, ****P*<0.0001; LGE: t_{10} = 9.561, ****P*<0.0001). TUNEL (t_{10} = 7.296, ****P*<0.0001). (h) The number of cleaved caspase-3/phospho-histone H3 double-positive cells was increased in the *Arid1b*^{+/-} MGE at E14.5 (t_{18} = 4.667, ****P*= 0.0002). N= 10 mice for each genotype. Statistical significance

was determined by a two-tailed Student's *t* test. **(i)** MGE primary cells were cultured from E12.5 *Arid1b*^{+/+} and *Arid1b*^{+/-} mice for 2 days. The cells were then incubated with 10 μM BrdU for 24 hours, fixed and immunostained with cleaved caspase-3 and BrdU antibodies. Scale bar= 40 μm. **(j)** Quantification of **i**. N= 6 cell culture replicates using 6 mice for each condition; cell counts= 1023 cells for *Arid1b*^{+/+} and 646 cells for *Arid1b*^{+/-}. Statistical significance was determined by a two-tailed Student's *t* test. Cleaved caspase-3 ($t_{10}= 2.419$, **P*= 0.0361). BrdU ($t_{10}= 3.520$, ***P*= 0.0055). **(k)** After 2 days of MGE culture, the TUNEL assay was performed. Scale bar= 40 μm. **(l)** Quantification of TUNEL-positive cells. Apoptosis was increased in *Arid1b* mutant cells ($t_{10}= 6.982$, ****P*= 0.0001). N= 6 cell culture replicates using 6 mice for each condition; cell counts= 598 cells for *Arid1b*^{+/+} and 605 cells for *Arid1b*^{+/-}. Statistical significance was determined by a two-tailed Student's *t* test. Data shown are the mean ± SEM.

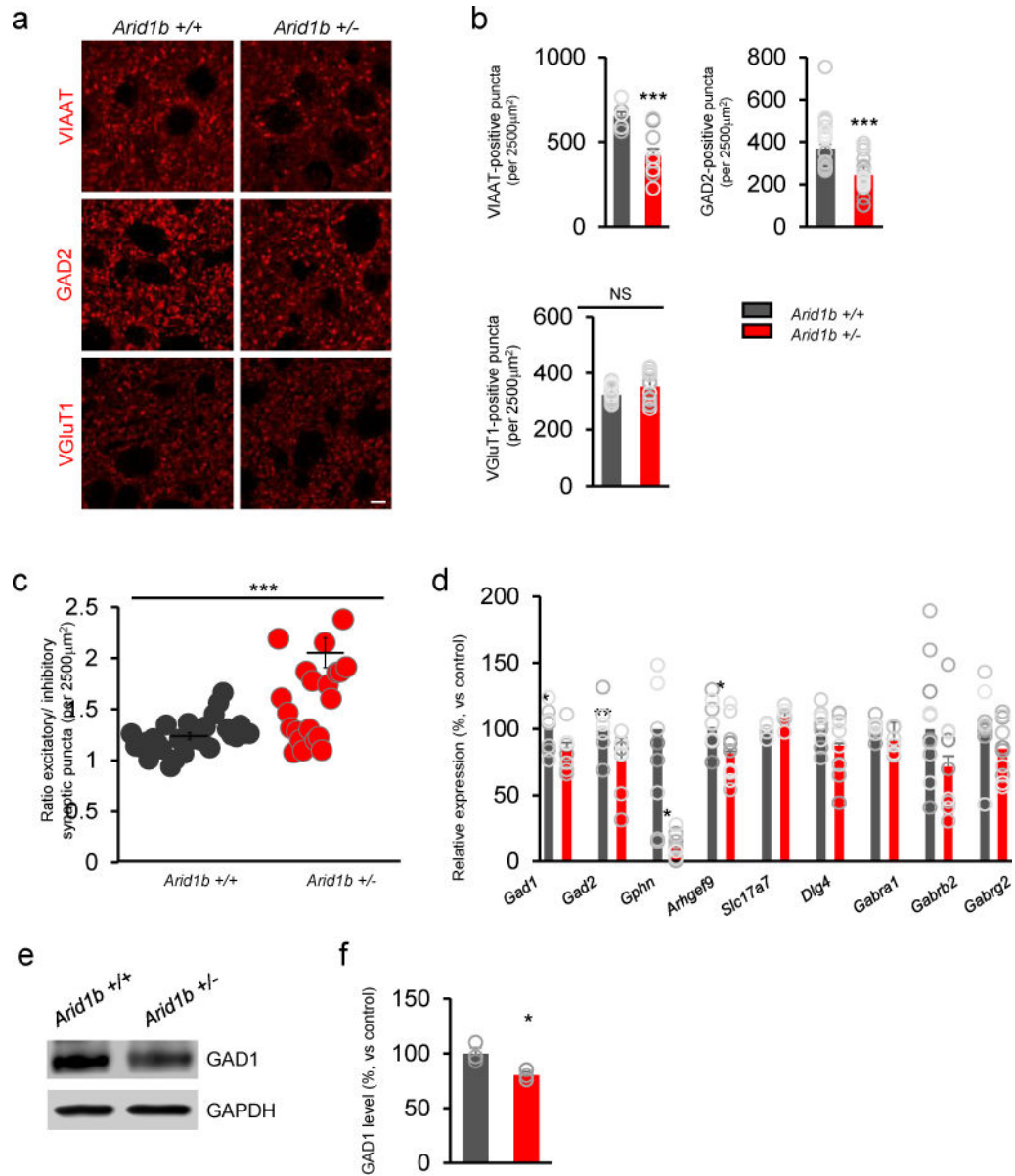


Figure 3. Altered synapses in *Arid1b*^{+/-} mice

The number of inhibitory synapses was reduced in *Arid1b*^{+/-} mice. **(a)** Inhibitory and excitatory synapses in P91 *Arid1b*^{+/+} and *Arid1b*^{+/-} cortices were examined by immunostaining using antibodies to inhibitory presynaptic markers VIAAT and GAD2 and an excitatory presynaptic marker VGluT1. Scale bar= 5 μm. **(b)** Quantification of **a**. The numbers of VIAAT - and GAD2-positive synaptic puncta were decreased in *Arid1b*^{+/-} mice at P91, while the number of excitatory presynaptic puncta was not different. VIAAT staining ($t_{18}= 4.823$, *** $P= 0.0001$): N= 10 mice for *Arid1b*^{+/+} (8 males, 2 females) and *Arid1b*^{+/-} (7 males, 3 females). GAD2 staining ($t_{44}= 4.226$, *** $P= 0.0001$): N= 23 mice for *Arid1b*^{+/+} (13 males, 10 females) and *Arid1b*^{+/-} (14 males, 9 females); VGluT1 staining: N= 15 mice for *Arid1b*^{+/+} (7 males, 8 females) and *Arid1b*^{+/-} (7 males, 8 females). Statistical significance was determined by a two-tailed Student's *t* test. NS: no significance. **(c)** A dot

plot shows the ratio of VGluT1-positive to VIAAT-positive puncta measured in **a** and **b**. Histogram shows the puncta ratio per 2500 μm^2 area in the cortex. There was an increase in this ratio in *Arid1b*^{+/-} cortical samples ($t_{54} = 4.435$, *** $P < 0.0001$). N= 28 mice for *Arid1b*^{+/+} (15 males, 13 females) and *Arid1b*^{+/-} (14 males, 14 females). Statistical significance was determined by a two-tailed Student's *t* test. **(d)** The mRNA levels of *Gad1*, *Gad2*, *Gphn*, *Arhgef9*, *Slc17a7*, *Dlg4*, *Gabra1*, *Gabrb2* and *Gabrg2* were assessed in P91 *Arid1b*^{+/+} and *Arid1b*^{+/-} cortical tissues by using real-time PCR (*Gad1*: $t_{18} = 2.709$, * $P = 0.0144$; *Gad2*: $t_{18} = 2.960$, ** $P = 0.0084$; *Gphn*: $t_{18} = 3.865$, ** $P = 0.0011$; *Arhgef9*: $t_{18} = 2.506$, * $P = 0.0201$). N= 10 independent experiments using 10 mice for each group. Statistical significance was determined by a two-tailed Student's *t* test. **(e)** Western blotting with an antibody to GAD1 was performed using cortical lysates from P91 *Arid1b*^{+/+} and *Arid1b*^{+/-} mice. **(f)** Quantification of **e**. N= 3 independent experiments using 6 mice for each group ($t_4 = 3.424$, * $P = 0.0367$). The intensity of protein and mRNA was normalized to the GAPDH level. Data were shown as relative changes versus *Arid1b*^{+/+} controls. Statistical significance was determined by a two-tailed Student's *t* test. Data shown are the mean \pm SEM.

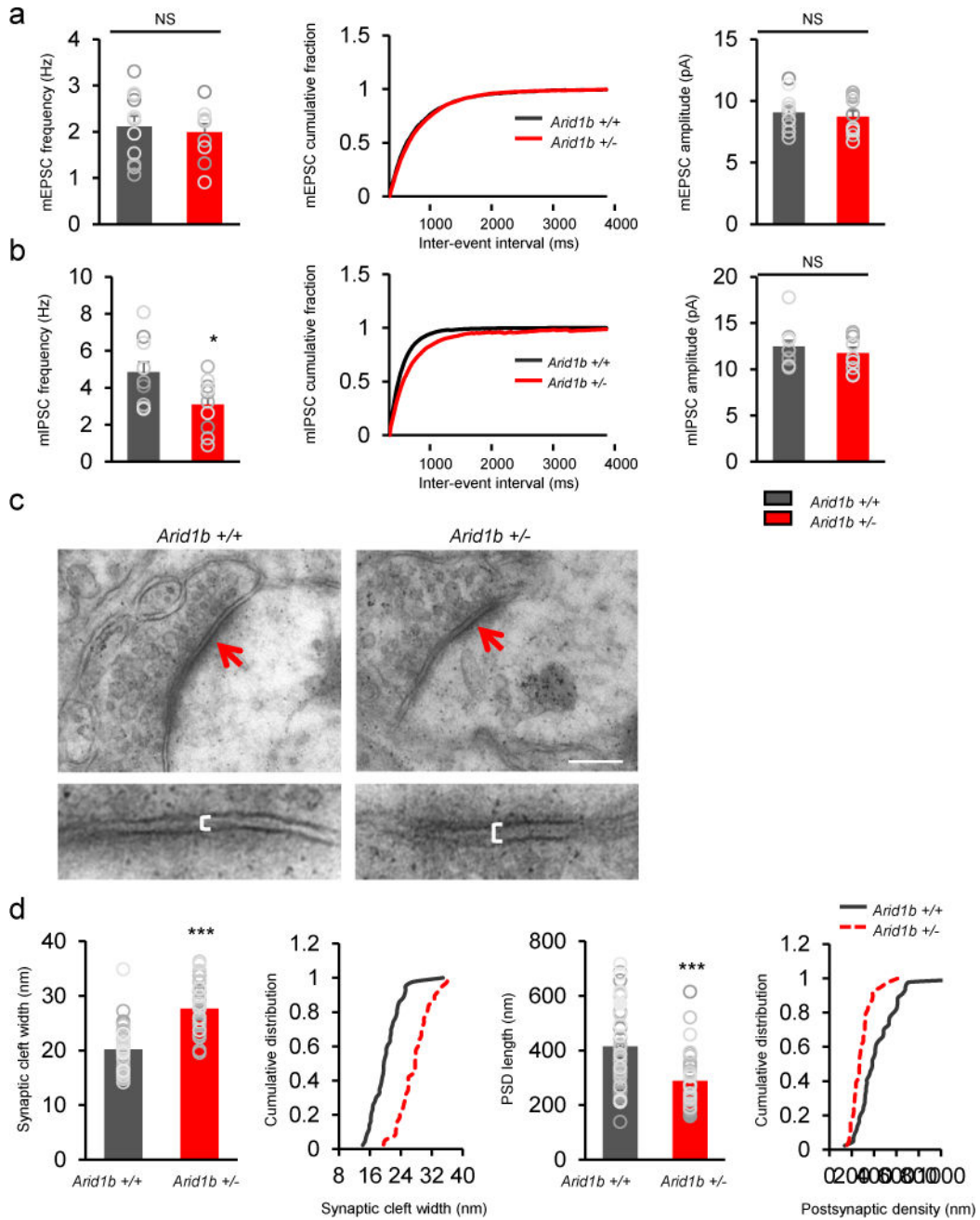
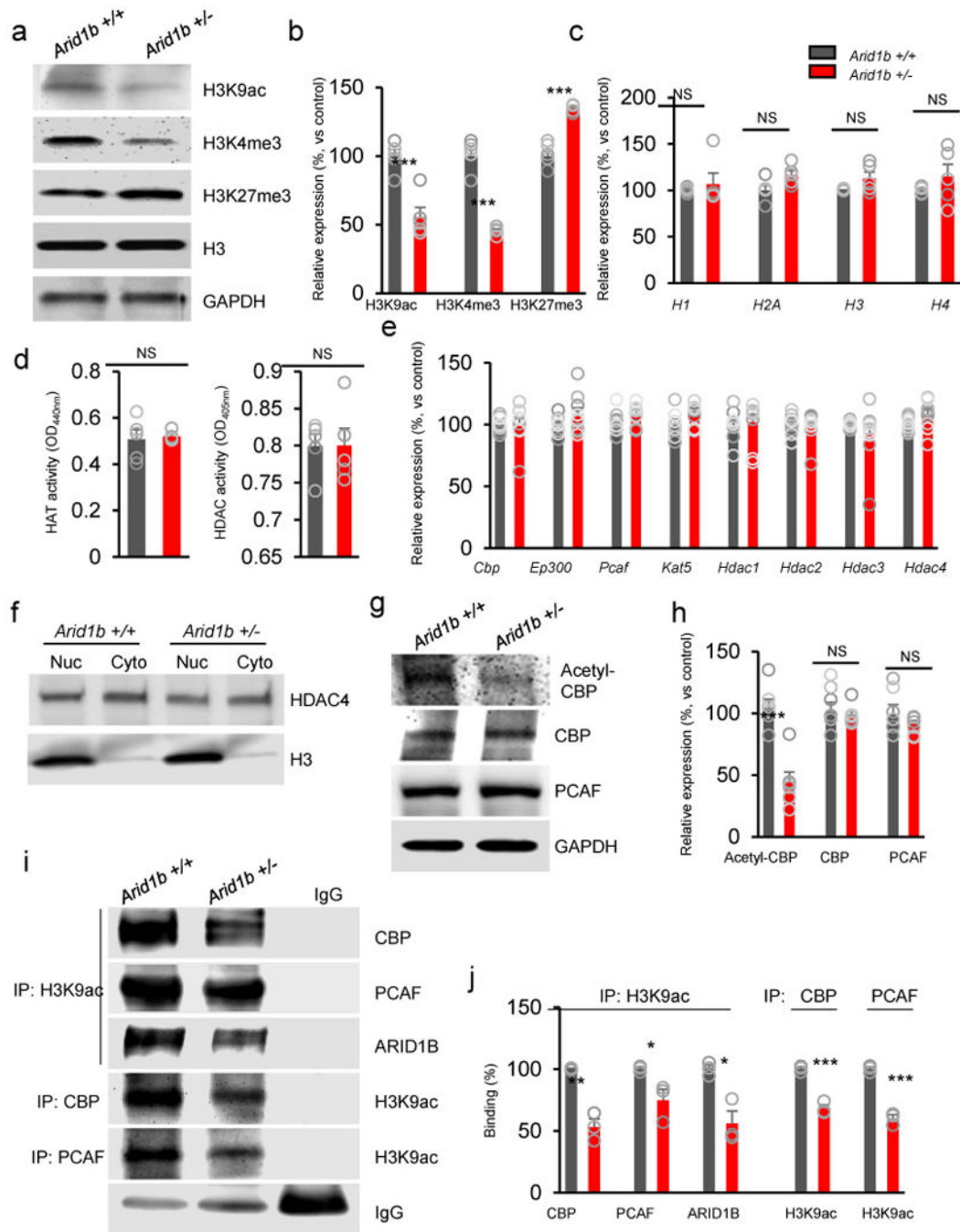


Figure 4. Postsynaptic currents and ultrastructure of inhibitory synapses in *Arid1b*^{+/-} mice
(a) Histograms show that mEPSC frequency, mEPSC amplitude, and mEPSC cumulative probability plot of inter-event interval were not significantly changed in *Arid1b*^{+/-} cortical slices compared with *Arid1b*^{+/+} cortical slices. Recordings were performed at -70 mV. Data were filtered at 2 kHz (1 kHz for presentation) and digitized at 20 kHz. N= 10 cells from 3 independent experiments using 3 mice for each condition. Statistical significance was determined by a two-tailed Student's *t* test. NS: no significance. **(b)** Histograms show quantification of mIPSC frequency, mIPSC amplitude, and mIPSC cumulative probability plot of inter-event interval. Decreased frequency of mIPSC was observed in *Arid1b*^{+/-}

cortical slices. Inter-event interval of mIPSCs was increased in *Arid1b*^{+/-} cortical slices. Recordings were performed at 0 mV. Data were filtered at 2 kHz (1 kHz for presentation) and digitized at 20 kHz. N= 10 cells from 3 independent experiments using 3 mice for each condition ($t_{18}= 2.447$, * $P= 0.0249$). Statistical significance was determined by a two-tailed Student's *t* test. NS: no significance. (c) Electron micrographs of inhibitory (symmetric) synapses (red arrows) in P91 *Arid1b*^{+/+} and *Arid1b*^{+/-} mice (top panels). Scale bar= 250 μm . Higher magnification images were shown in bottom panels (white bars indicate cleft width). Scale bar= 25 μm . (d) Quantification of the synaptic cleft width and the postsynaptic density length. The width of synaptic clefts was increased in *Arid1b*^{+/-} synapses while the postsynaptic density length was decreased. Synaptic cleft width ($t_{77}= 8.456$, *** $P<0.0001$): N= 43 and 44 synapses using 3 mice for *Arid1b*^{+/+} and *Arid1b*^{+/-}, respectively. Synaptic density length ($t_{80}= 4.522$, *** $P<0.0001$): N= 38 and 42 synapses using 3 mice for *Arid1b*^{+/+} and *Arid1b*^{+/-}, respectively. Statistical significance was determined by a two-tailed Student's *t* test. Data shown are the mean \pm SEM.



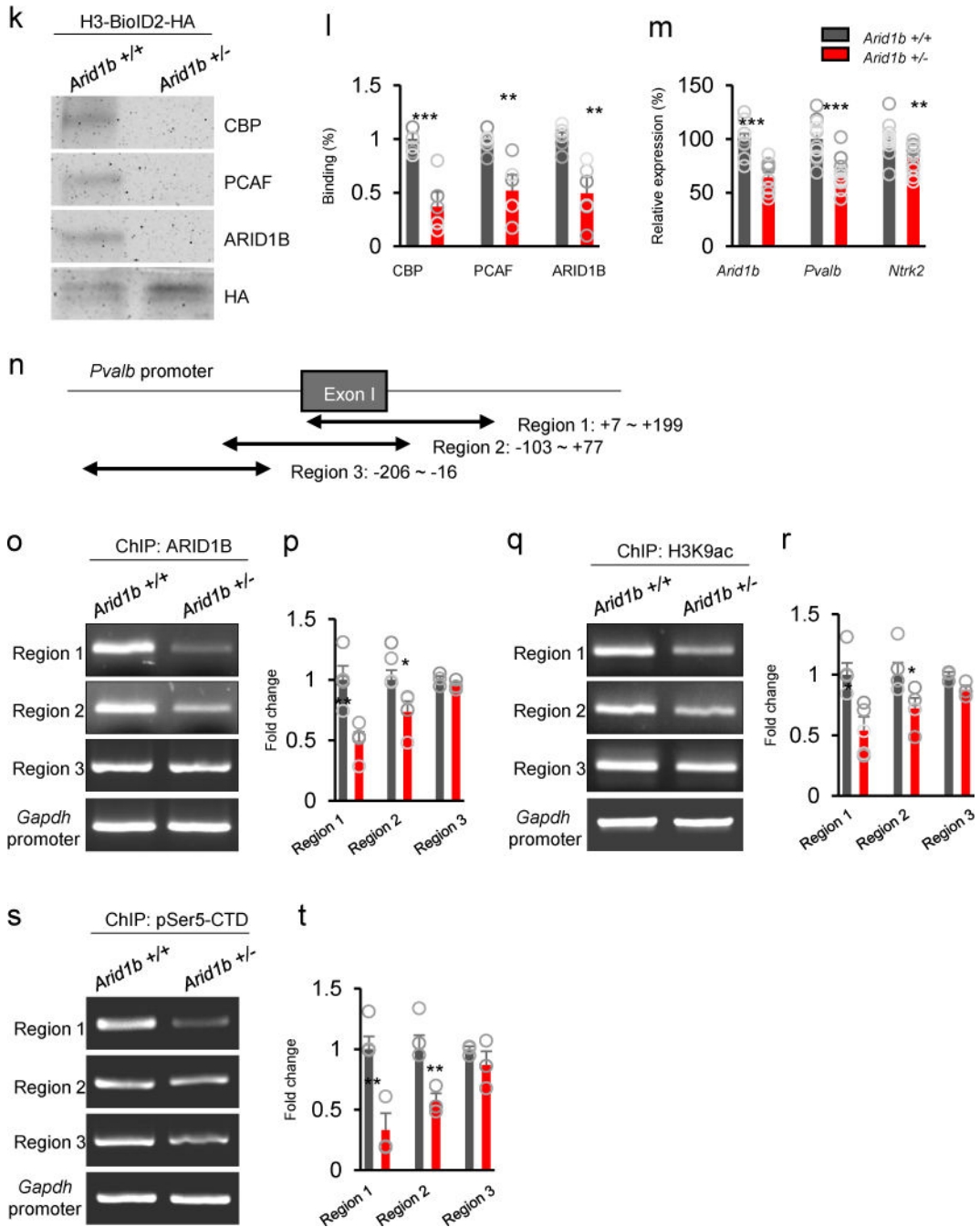
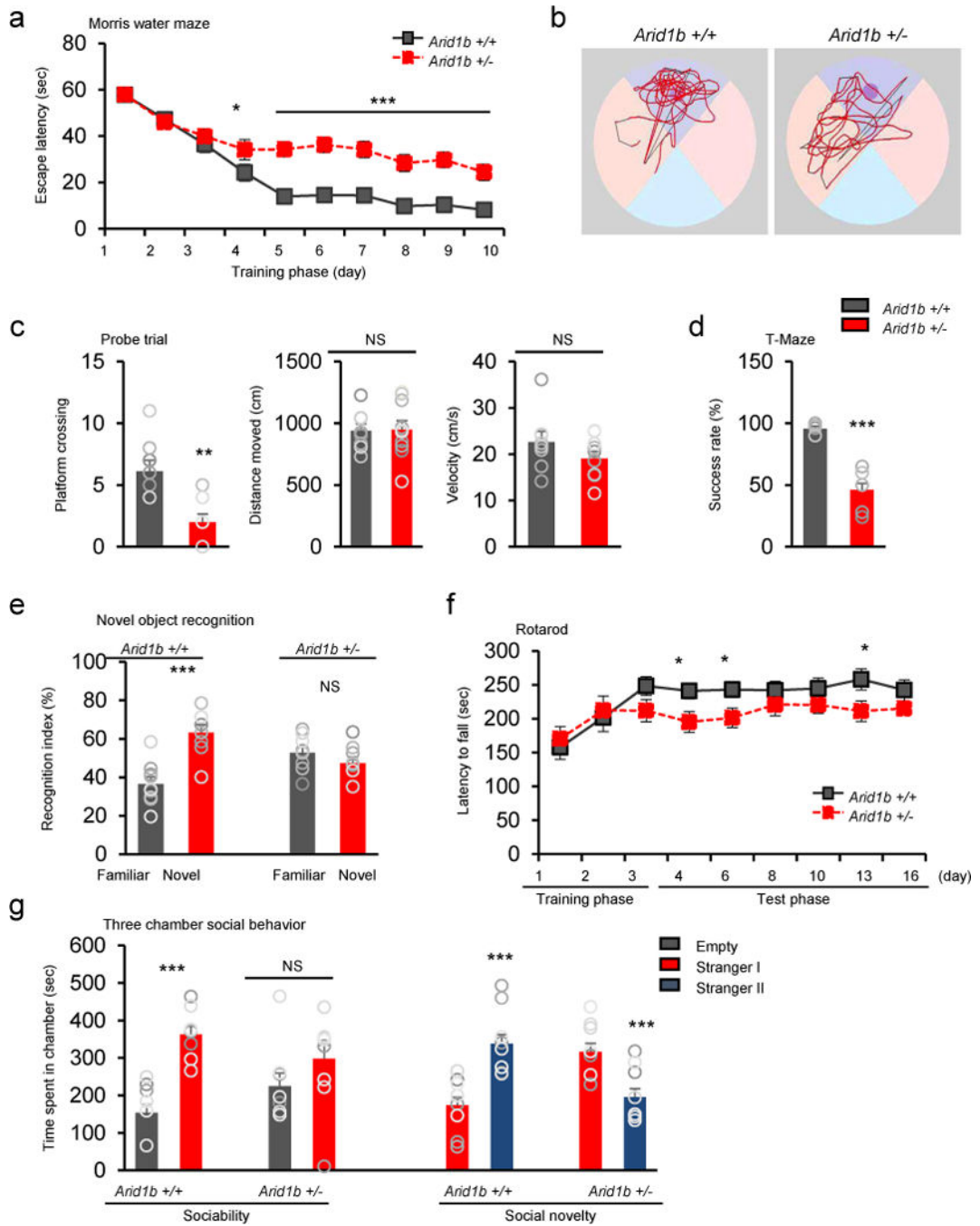


Figure 5. *Arid1b* regulates histone acetylation on the *Pvalb* promoter

(a) Western blots show altered histone acetylation and methylation in *Arid1b*^{+/-} cortices. (b) Quantification of a. The band intensity of each protein was normalized to the GAPDH level. Histone H3 acetylation at K9: $t_8 = 5.163$, *** $P = 0.0009$. Histone H3 trimethylation at Lysine 4: $t_8 = 10.60$, *** $P < 0.0001$. Histone H3 trimethylation at Lysine 27: $t_8 = 8.325$, *** $P < 0.0001$. $N = 5$ independent experiments using 5 mice for each genotype. Statistical significance was determined by a two-tailed Student's *t* test. (c) The mRNA levels of histone genes were assessed by using real-time PCR in cortical tissues of P91 *Arid1b*^{+/+} and *Arid1b*^{+/-} mice.

N= 5 independent experiments using 5 mice for each group. The level of *Gapdh* mRNA was used for normalization. Data were shown as relative changes in *Arid1b*^{+/-} versus *Arid1b*^{+/+} control samples. Statistical significance was determined by a two-tailed Student's *t* test. NS: no significance. **(d)** The activities of HATs and HDACs showed no changes in *Arid1b*^{+/-} cortices. N= 5 independent experiments using 5 mice for each genotype. Statistical significance was determined by a two-tailed Student's *t* test. NS: no significance. **(e)** The mRNA levels of *Hat* and *Hdac* genes were assessed using real-time PCR in cortical tissues of P91 *Arid1b*^{+/+} and *Arid1b*^{+/-} mice. The levels of mRNAs for histone genes were normalized to the *Gapdh* mRNA levels. Data were shown as relative changes in *Arid1b*^{+/-} versus *Arid1b*^{+/+} samples. N= 9 independent experiments using 9 mice for each group. Statistical significance was determined by a two-tailed Student's *t* test. No significance was found for each comparison. **(f)** Western blotting for HDAC4 using nuclear (Nuc) and cytoplasmic (Cyto) extracts prepared from *Arid1b*^{+/+} and *Arid1b*^{+/-} cortices. Histone H3 was used as a nuclear marker. **(g)** Western blotting showed that the level of acetyl-CBP was decreased, while CBP and PCAF protein levels were not changed in *Arid1b*^{+/-} cortices. **(h)** Quantification of **g**. The band intensity of each protein was normalized to the GAPDH level ($t_{10}= 5.521$, *** $P= 0.0003$). N= 6 independent experiments using 6 mice for each condition. Statistical significance was determined by a two-tailed Student's *t* test. NS: no significance. **(i)** Co-immunoprecipitation experiments showed the association of H3K9ac with CBP, PCAF, and ARID1B in cortices. **(j)** Quantification of **i**. H3K9ac with CBP: $t_4= 7.252$, ** $P= 0.0019$. H3K9ac with PCAF: $t_4= 2.883$, * $P= 0.0472$. H3K9ac with ARID1B: $t_4= 4.230$, * $P= 0.0134$. CBP with H3K9ac: $t_4= 10.05$, *** $P= 0.0006$. PCAF with H3K9ac: $t_{10}= 12.64$, *** $P= 0.0002$. N= 3 independent experiments using 3 mice for each condition. Statistical significance was determined by a two-tailed Student's *t* test. **(k)** The BioID2 assay shows histone H3 interaction with CBP, PCAF, and ARID1B. **(l)** Quantification of **k**. CBP: $t_{10}= 7.378$, *** $P<0.0001$. PCAF: $t_{10}= 4.095$, ** $P= 0.0022$. ARID1B: $t_{10}= 4.496$, ** $P= 0.0011$. N= 6 independent experiments using 6 mice for each condition. Statistical significance was determined by a two-tailed Student's *t* test. **(m)** Real-time PCR showed *Pvalb* and *Ntrk2* mRNA levels in *Arid1b*^{+/-} cortices. *Arid1b*: $t_{20}= 5.021$, *** $P= 0.0001$. *Pvalb*: $t_{20}= 4.722$, *** $P= 0.0001$. *Ntrk2*: $t_{20}= 3.123$, ** $P= 0.0054$. N= 11 independent experiments using 11 mice for each genotype. Statistical significance was determined by a two-tailed Student's *t* test. **(n)** A schematic drawing showing the *Pvalb* gene promoter regions examined by ChIP-qPCR. **(o)** The ChIP-qPCR assay showed that ARID1B to the *Pvalb* promoter was decreased in *Arid1b*^{+/-} cortices. **(p)** Quantification of **o**. Region 1: $t_6= 3.710$, ** $P= 0.01$. Region 2: $t_6= 3.187$, * $P= 0.0189$. N= 4 independent experiments using 4 mice for each condition. Statistical significance was determined by a two-tailed Student's *t* test. **(q)** The ChIP-qPCR assay showed that the association of H3K9ac with the *Pvalb* promoter was decreased in *Arid1b*^{+/-} cortices. **(r)** Quantification of **q**. Region 1: $t_6= 3.274$, * $P= 0.017$. Region 2: $t_6= 2.510$, * $P= 0.0459$. N= 4 independent experiments using 4 mice for each condition. Statistical significance was determined by a two-tailed Student's *t* test. **(s)** The ChIP-qPCR assay showed that the association of RNA polymerase II phospho-CTD (Ser5) with the *Pvalb* promoter was decreased in *Arid1b*^{+/-} cortices. **(t)** Quantification of **s**. Region 1: $t_6= 5.916$, ** $P= 0.001$. Region 2: $t_6= 5.237$, ** $P= 0.0019$. N= 4 independent experiments using 4 mice for each condition. Statistical significance was determined by a two-tailed Student's *t* test. Data shown are the mean \pm SEM.



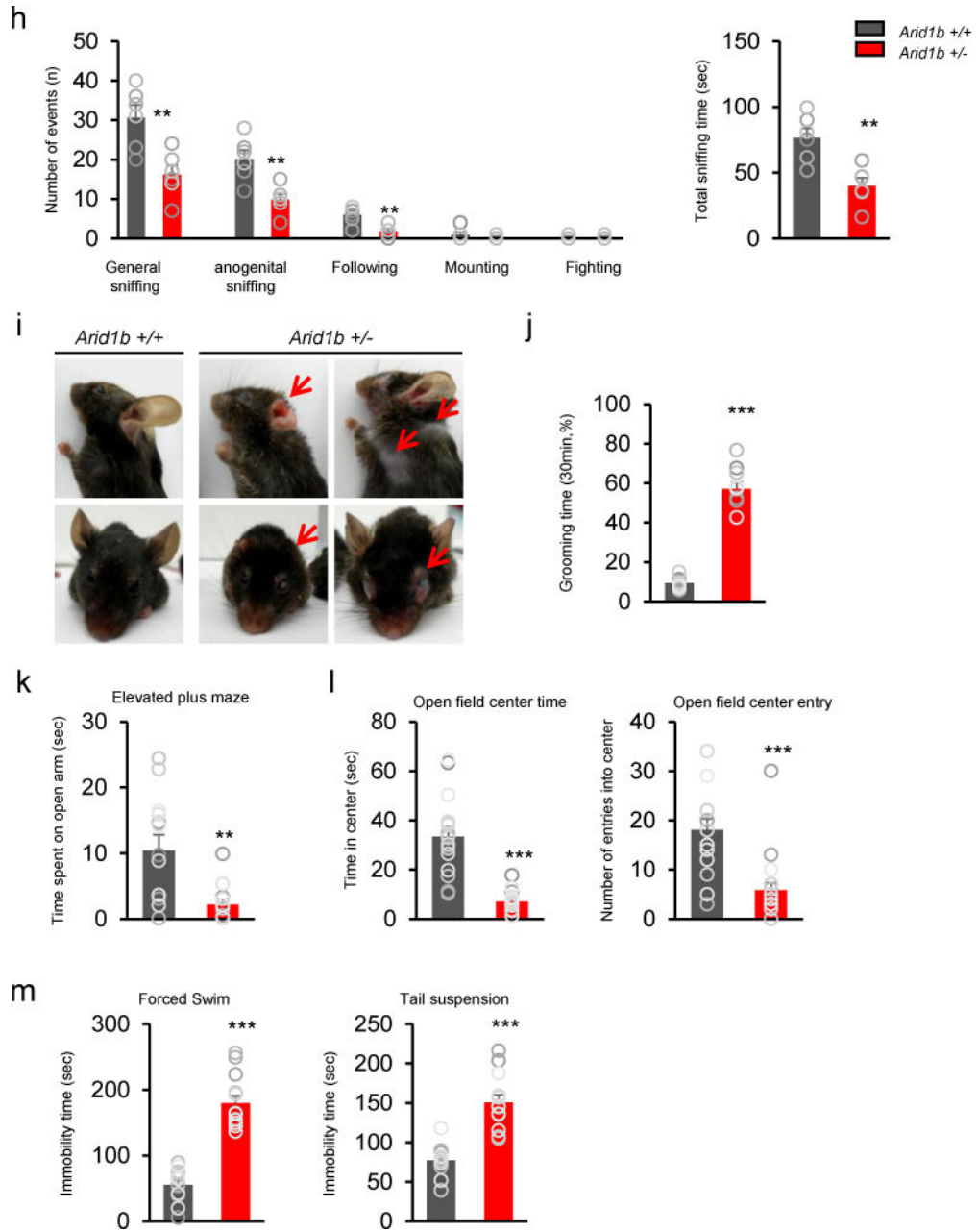


Figure 6. *Arid1b*^{+/-} mice show impaired cognitive and social behavior

(a) The Morris water maze assay shows spatial learning disability in *Arid1b*^{+/-} mice. 4 days: $t_{70} = 2.031$, $*P = 0.0463$. 5 days: $t_{70} = 4.977$, $***P < 0.0001$. 6 days: $t_{70} = 5.397$, $***P < 0.0001$. 7 days: $t_{70} = 4.374$, $***P < 0.0001$. 8 days: $t_{70} = 4.270$, $***P < 0.0001$. 9 days: $t_{70} = 4.928$, $***P < 0.0001$. 10 days: $t_{70} = 3.932$, $***P = 0.0002$. N= 8 mice (4 male, 4 female) for *Arid1b*^{+/+} and 10 mice (5 male, 5 female) for *Arid1b*^{+/-}. Statistical significance was determined by a two-tailed Student's *t* test. (b) Representative swim paths of *Arid1b*^{+/+} and *Arid1b*^{+/-} mice during a probe trial after training. (c) Quantification of b. *Arid1b*^{+/-} mice showed a decrease in platform crossings ($t_{16} = 3.868$, $**P = 0.0014$). Statistical significance was determined by a two-tailed Student's *t* test. NS: no significance. (d) In the T-maze test,

the success rate of food retrieval in *Arid1b*^{+/-} mice was decreased compared with *Arid1b*^{+/+} mice ($t_{10}=6.991$, *** $P<0.0001$). $N=6$ mice (3 males, 3 females) for each genotype. Statistical significance was determined by a two-tailed Student's t test. (e) The novel object recognition test was performed. $t_{15}=4.749$, *** $P=0.0003$. $N=9$ (5 males, 4 females) for *Arid1b*^{+/+} mice; $N=8$ (5 males, 3 females) for *Arid1b*^{+/-} mice. Statistical significance was determined by a two-tailed Student's t test. NS: no significance. (f) In the rotarod test, the latency to fall during test phases was reduced in *Arid1b*^{+/-} mice. 4 days: $t_{34}=2.359$, * $P=0.0242$. 6 days: $t_{34}=2.198$, * $P=0.0353$. 13 days: $t_{34}=2.141$, * $P=0.0397$. $N=6$ mice (3 males, 3 females) for each genotype. Statistical significance was determined by a two-tailed Student's t test. (g) Using the three-chamber paradigm, the sociability test was performed in *Arid1b*^{+/+} and *Arid1b*^{+/-} mice. $t_{20}=6.313$, *** $P<0.0001$. In the social novelty test, *Arid1b*^{+/-} mice spent less time with the novel mouse (stranger II) than with the familiar mouse (Stranger I). *Arid1b*^{+/+}: $t_{20}=4.874$, *** $P<0.0001$. *Arid1b*^{+/-}: $t_{22}=4.900$, *** $P<0.0001$. $N=11$ male mice for *Arid1b*^{+/+} and 12 male mice for *Arid1b*^{+/-}. Statistical significance was determined by a two-tailed Student's t test. NS: no significance. (h) Social interaction was performed using an open field apparatus. *Arid1b*^{+/-} mice showed decreased interaction compared with *Arid1b*^{+/+} mice (left panel). Sniffing: $t_{10}=3.678$, ** $P=0.0043$. Anogenital sniffing: $t_{10}=3.872$, ** $P=0.0031$. Following: $t_{10}=0.867$, ** $P=0.0031$. The right panel shows quantification of total sniffing time ($t_{10}=3.896$, ** $P=0.0033$). $N=6$ male mice for each genotype. Statistical significance was determined by a two-tailed Student's t test. (i) Excessive grooming leads to severe facial, neck, and shoulder lesions in *Arid1b*^{+/-} mice (red arrows). (j) *Arid1b*^{+/-} mice showed increased grooming time compared with *Arid1b*^{+/+} mice ($t_{18}=13.64$, *** $P<0.0001$). $N=10$ mice for *Arid1b*^{+/+} (6 males, 4 females) and *Arid1b*^{+/-} (5 males, 5 females). Statistical significance was determined by a two-tailed Student's t test. (k) In the elevated plus maze test, *Arid1b*^{+/-} mice spent less time in the open arms ($t_{23}=3.251$, ** $P=0.0035$). $N=13$ mice (7 males, 6 females) for *Arid1b*^{+/+} and 12 mice (6 males, 6 females) for *Arid1b*^{+/-}. Statistical significance was determined by a two-tailed Student's t test. (l) The time spent in the center and the numbers of entries into the center were examined in the open field. Open field center time: $t_{34}=7.189$, *** $P<0.0001$. Open field center entries: $t_{34}=4.713$, *** $P<0.0001$. $N=16$ mice (9 males, 7 females) for *Arid1b*^{+/+} and 20 mice (11 males, 9 females) for *Arid1b*^{+/-}. Statistical significance was determined by a two-tailed Student's t test. (m) In both the forced swim test and the tail suspension test, the immobility time was increased in *Arid1b*^{+/-} mice. Forced swim test: $t_{23}=9.169$, *** $P<0.0001$. Tail suspension test: $t_{23}=6.416$, *** $P<0.0001$. $N=12$ mice (7 males, 5 females) for *Arid1b*^{+/+} and 13 mice (7 males, 6 females) for *Arid1b*^{+/-}. Statistical significance was determined by a two-tailed Student's t test. Data shown are the mean \pm SEM.

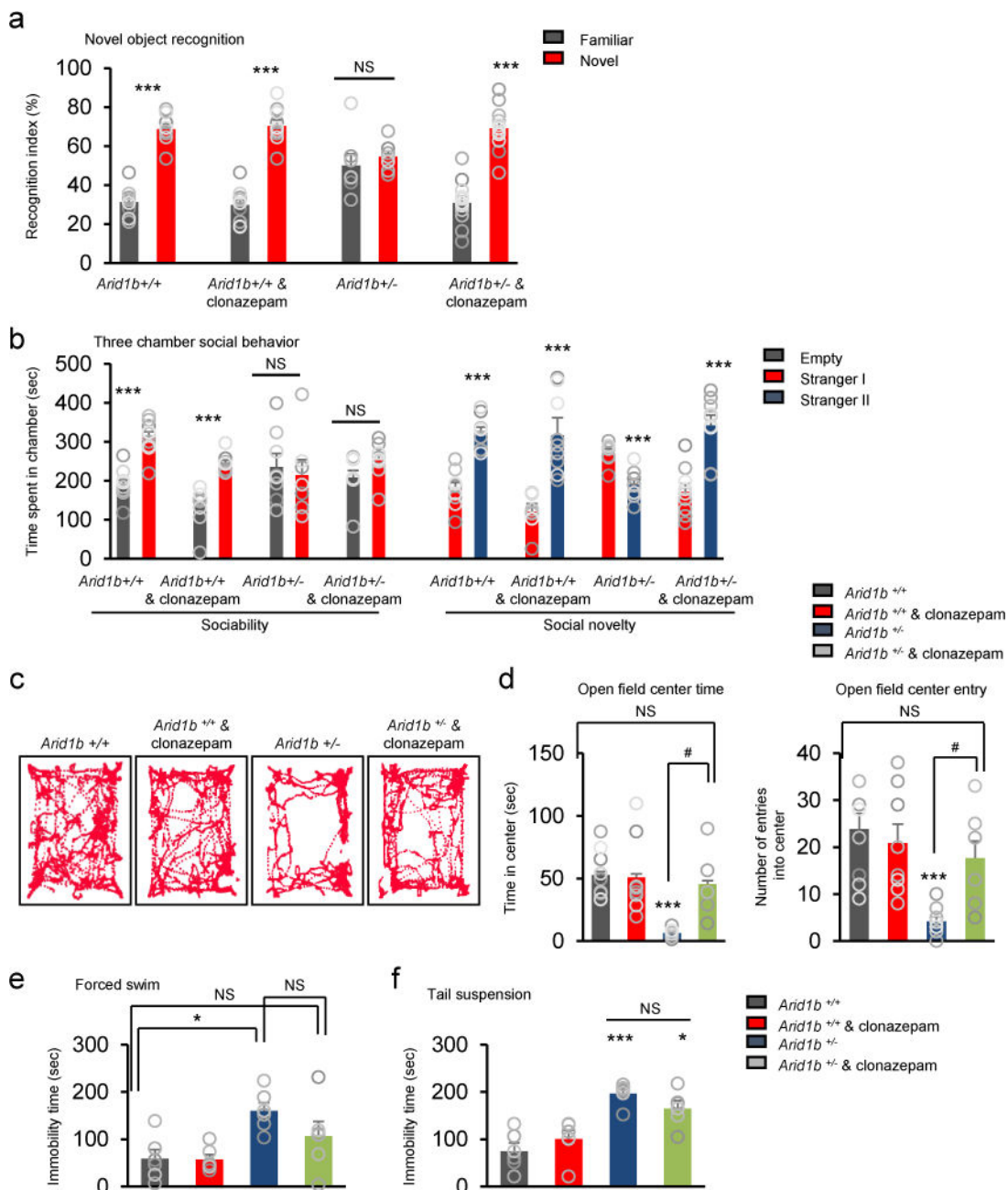


Figure 7. Activation of GABA signaling rescues abnormal behaviors in *Arid1b*^{+/-} mice
(a) Increase in the GABA tone reverses recognition memory deficits in *Arid1b*^{+/-} mice. Either saline or 0.0625 mg/kg clonazepam was administered to control and *Arid1b*^{+/-} mice intraperitoneally, followed by the object recognition test. Saline-treated *Arid1b*^{+/+}: $t_{14} = 9.402$, *** $P < 0.0001$. Clonazepam-treated *Arid1b*^{+/+}: $t_{20} = 11.34$, *** $P < 0.0001$. Clonazepam-treated *Arid1b*^{+/-}: $t_{22} = 8.345$, *** $P < 0.0001$. $N = 8$ mice (5 males, 3 females) for saline-treated *Arid1b*^{+/+}, 10 mice (7 males, 3 females) for clonazepam-treated *Arid1b*^{+/+}, $N = 7$ mice (5 males, 2 females) for saline-treated *Arid1b*^{+/-}, and 10 mice (6 males, 4 females) for clonazepam-treated *Arid1b*^{+/-}. Statistical significance was determined by a two-tailed Student's *t* test. NS: no significance. **(b)** In the sociability test, clonazepam-

treated *Arid1b*^{+/-} mice had no preference for either chamber. Saline-treated *Arid1b*^{+/+}: $t_{16}=6.082$, *** $P<0.0001$. Clonazepam-treated *Arid1b*^{+/+}: $t_{16}=6.153$, *** $P<0.0001$. However, the social novelty test showed that social memory in *Arid1b*^{+/-} mice was restored by clonazepam treatment. Saline-treated *Arid1b*^{+/+}: $t_{16}=6.767$, *** $P<0.0001$. Clonazepam-treated *Arid1b*^{+/+}: $t_{16}=5.355$, *** $P<0.0001$. Saline-treated *Arid1b*^{+/-}: $t_{16}=5.170$, *** $P=0.0001$. Clonazepam-treated *Arid1b*^{+/-}: $t_{16}=5.124$, *** $P=0.0001$. N= 9 male mice for saline-treated *Arid1b*^{+/+}, 9 male mice for clonazepam-treated *Arid1b*^{+/+}, 7 male mice for saline-treated *Arid1b*^{+/-}, and 9 male mice for clonazepam-treated *Arid1b*^{+/-}. Statistical significance was determined by a two-tailed Student's *t* test. NS: no significance. (c) Representative tracing of mouse movement in the open field test. (d) Quantification of c. Open field center time: $F_{3,28}=8.89$, *** $P<0.0001$ for saline-treated *Arid1b*^{+/+} versus saline-treated *Arid1b*^{+/-}; # $P<0.05$ for saline-treated *Arid1b*^{+/-} versus clonazepam-treated *Arid1b*^{+/-}. Center entries: $F_{3,28}=7.668$, *** $P<0.0001$ for saline-treated *Arid1b*^{+/+} versus saline-treated *Arid1b*^{+/-}; # $P<0.05$ for saline-treated *Arid1b*^{+/-} versus clonazepam-treated *Arid1b*^{+/-}. N= 9 mice (6 males, 3 females) for saline-treated *Arid1b*^{+/+}, 8 mice (5 males, 3 females) for clonazepam-treated *Arid1b*^{+/+}; 9 mice (6 males, 3 females) for saline-treated *Arid1b*^{+/-}, and 6 mice (5 males, 1 female) for clonazepam-treated *Arid1b*^{+/-}. Statistical significance was determined by one-way ANOVA with the Bonferonni correction test. NS: no significance. (e and f) Immobility time was measured in *Arid1b*^{+/+} and *Arid1b*^{+/-} mice by the forced swim test (e) or the tail suspension test (f). Forced swim test: $F_{3,20}=5.605$, * $P<0.05$ for saline-treated *Arid1b*^{+/+} versus saline-treated *Arid1b*^{+/-}. Tail suspension test: $F_{3,20}=14.8$, *** $P<0.0001$ for saline-treated *Arid1b*^{+/+} versus saline-treated *Arid1b*^{+/-}; * $P<0.05$ for saline-treated *Arid1b*^{+/+} versus clonazepam-treated *Arid1b*^{+/-}. N= 6 mice (3 males, 3 females) for saline-treated *Arid1b*^{+/+}, 6 mice (4 males, 2 females) for clonazepam-treated *Arid1b*^{+/+}, 6 mice (3 males, 3 females) for saline-treated *Arid1b*^{+/-}, and 6 mice (5 males, 1 female) for clonazepam-treated *Arid1b*^{+/-}. Statistical significance was determined by one-way ANOVA with the Bonferonni correction test. NS: no significance. Data shown are the mean \pm SEM.